Application and comparison of high resolution radiation models in complex terrain

Chris Marsh

Geography 490

April 2009

Table of contents

Contents

1. INTRODUCTION

Computer aided simulations are important for helping understand the complex interactions present in nature and improving our understanding of both climate and hydrologic systems (Liston and Elder 2006). Simulation models are also a way to encapsulate our knowledge of natural systems, and therefore provide a method to test our understanding of nature. In addition, they help predict a variety of important phenomenon ranging from understanding the details of segments of the hydrologic system such as the effects of vegetation on hydrologic systems, to more general consideration of the impacts of anthropogenic changes on water resources. In order to utilize simulation models, it is also imperative to have observations of key aspects of both the atmospheric and hydrologic. Unfortunately, there has been a systematic reduction in density of measuring locations for many atmospheric and hydrological variables in many areas of the world, including Canada. Simultaneously, there has been a reduced measuring capacity at each location. In terms of the Canadian observation system, this has been termed "[…] a national disgrace" (Shook and Pomeroy 2008). Since current generation, high resolution hydrologic and atmospheric models require scale-appropriate atmospheric forcing variables (Liston and Elder 2006), this decrease in observation density has resulted in a reduction of the data available to run and test numerical models. As a result, there is a reduced capacity to predict both past and future events at high temporal and spatial resolutions. Even with a very dense meteorological station network, there is a need to utilize methods that estimate important forcing variables at a point and distribute these variables over the domain of interest. It is also possible to estimate certain difficult to obtain variables from other, easily obtained variables. As one example, it has been observed that atmospheric transmittance can be estimated from daily temperature variations and precipitation (Bristow and Campbell 1985; Bristow and Campbell 1984).

In addition to the above noted atmospheric forcing data, and depending on the modeling objectives, it is typically necessary to use high resolution topographic data. Previously, such topographic information was not readily available; however, with the advent of airborne mapping technologies such as LiDAR, high resolution digital elevation models (DEM) have become available allowing for increased resolution in spatial modeling. As a result it is possible, where appropriate, to consider spatial variations on smaller and smaller spatial scales. One effect of increase in spatial resolution is that such high resolution modeling requires an increase in computing power to solve the controlling equations. Although an increase in spatial resolution brings with it a potential for increased accuracy, it does bring with it additional complexities. For example it is often not known what an "ideal" scale is to correctly model certain processes; different approximating equations and methods may only be applicable at certain scales (spatial or temporal), and various additional parameters (i.e. soil hydraulic conductivity) may also be required at this fine scale. However, such parameters may not be available at the required resolution due

to geographic, financial and man power limitations. Therefore, an ability to interpolate variables as a function of their distance from a given observation is desirable.

There are a variety of methods for spatial interpolation ranging from the numerically simple to numerically complex. Examples include: Inverse Distance Weighting (IDW), Kriging, 2-dimensional spline, trend surface and kernel estimators to name but a few (Myers 1993; Dodson and Marks 1997). Each method has various pros and cons, however the two most popular in the Earth sciences are Kriging, Spline (with and without tension) and IDW methods.

In order to correctly model almost all hydrologic processes, there is a need for data on air temperature, humidity and incoming direct and diffuse shortwave radiation, among other variables. One of the more difficult meteorological variables to estimate, and extremely important to many hydrological and atmospheric processes, is incoming solar radiation and solar radiation incident on slopes of various angles and aspects. As the radiation passes through the atmosphere, the energy partially scatters and is absorbed by atmospheric particulates such as water vapour, atmospheric gases, particulates and cloud droplets. The amount of radiation that reaches the earth after retardation effect of these on the amount of solar energy that is transmitted to the Earth's surface is referred to as the atmospheric transmittance. Unfortunately, the atmospheric transmittance is very difficult to measure and would require measurements of all of the atmospheric properties throughout the entire height of the atmosphere. However, many observations (Bristow and Campbell 1985; Bristow and Campbell 1984; Walter et al. 2005) have shown that such measurements are not necessarily required as a good relationship exists between transmittance, air temperature and relative humidity at a single level in the atmosphere. Other methods can be used without any atmospheric forcing data by using "average" or "common" values for variables, such as transmittance. An implementation of this is available in the ArcGIS 9.3 (as well as in previous versions) Spatial Analyst toolbox which can estimate point and grid incoming solar radiation (diffuse and direct) without the need for any atmospheric variables. Within this paper, a number of methods for calculating incoming shortwave radiation are examined. Two are empirically based; infinite plane approximations and two are quasi-physically based equations for application on sloping terrain (ie: shadowing and slope/aspect effects are taken into account). The empirical equations require very little driving data, needing only daily minimum and maximum air temperature to calculate daily transmittance values, while the physically based equations typically require additional data such as high resolution DEMs and requires addition computing to obtain solutions to "helping" equations such as zenith angles and optical air mass.

This research project will consider two spatial interpolation methods: thin plate spline with tension, a computationally expensive exact interpolate as well as a computationally quick method called Inverse Distance Weighting (IDW). Both methods have numerous benefits and downsides. IDW is

computationally fast, as well as trivial to implement from a programming aspect. However, it is bound on the minimum and maximum of the input data; that is to say, it can never exceed the minimum and maximums in the driving data set. Spline interpolation is not hampered by this limitation, and can provide data outside of the minimum, maximum bounds of the driving data set; however it requires considerable computing resources. Both methods are exact interpolates (defined below) which make them ideal for measured data points.

Hypothesis and questions:

This paper will consider the following questions and hypothesis related to estimating key atmospheric parameters required for high resolution radiation modeling in mountainous terrain:

Question 1:

Can temperature based, empirical shortwave radiation models generate useful approximations in complex terrain without the inclusion of a shading model?

Hypothesis 1:

Complex terrain is heavily shaded and since the models do not take into account shading, they will over estimate the incoming shortwave in these shaded locations. However, in open terrain they might still predict the results sufficiently accurately to allow application to other research topics such as snow melt.

Due to the heavy dependence of the empirical models on temperature, there will most likely be an under/over estimation in locations of high elevation if the interpolated temperature uses too low/high of a lapse rate. Therefore it will be dependent upon good temperature interpolation.

Question 2:

Is the compute-intensive spline method better than the simple IDW scheme for interpolating temperature and humidity? Will a poor interpolation destroy the results?

Hypothesis 2:

Due to the fact that spline takes into account the ‘weight’ of each measured point as defined by its distance from the known points, as well as providing a smoothing mechanism to account for wild overshoots, it should be able to be less sensitive to large fluctuations due to elevation changes and will potentially smooth out some of the instrument noise. It is anticipated that IDW will result in large wells that will distract from the realism of the interpolated data.

Question 3:

Are physically based methods, derived for other mountainous regions, applicable to the Rocky Mountains? Since the diffuse components have required some empirical calibration, they will be 'tuned' to the calibration site. How transferable these equations are to other mountains regions is of interest?

Hypothesis 3:

Although calibrated for other areas, it is expected that these models will work reasonably well given the somewhat similar nature of mountain ranges.

Question 4:

Is there a preference for the air temperature lapse rate that is used? Is a variable month lapse rate acceptable for the Rockies or should a different method be used, such as the potential temperature method?

Hypothesis 4:

Given that the atmospheric conditions over mountains are typically not stable, a method that assumes a stable atmosphere shouldn't work as well as a lapse rate. However due to cold air drainage, inversions and other phenomena, it might be a better assumption than a constant lapse rate for the model domain.

To address these questions, a variety of techniques for predicting atmospheric variables will be used and compared to measured data. Variables for prediction are:

i. Air temperature
ii. Humidity

Temperature and humidity will be interpolated using an variable and constant lapse rates and an IDW scheme as well as spline to compare the effectiveness of the more computationally intense method to that of the simple IDW scheme. These will be used to drive the radiation models. Results will be validated via cross validation

2. INTERPOLATION METHODS

2.2 Spatial Interpolation

Interpolation, in the context of earth sciences, is a method to estimate the values of an unknown function f where values of f are known at a finite number of points and where the objective is to produce an approximation to the value of f at a point where f is not known (Myers 1993). Interpolates may be

exact, such that if y is the known value at x, *f(x)=y*. Given that errors are present in the data collection, it may be acceptable to have a function *f* such that at a point x with a known value y, $f(x) = y + \delta y$, where δy is some difference between the known point and the point produced via *f*. These are termed non-exact interpolates.

There are many different methods that can be applied for spatial interpolation ranging from the simple to the complex. Examples of this are: Inverse Distance Weighting (IDW), Kriging, 2-dimensional spline, trend surface, kernel estimators and radial basis functions (Myers 1993; Dodson and Marks 1997; Chang 2008). When applied to geophysical processes, the choice of a spatial interpolator is very important where data collection sites are sparse and variables vary across short differences (Chung and Yun 2004). In such cases, a small bias resulting from an incorrectly chosen interpolate can lead to erroneous conclusions (Bolstad et al. 1998; Chung and Yun 2004).

2.2.1 Inverse Distance Weighted (IDW)

Inverse distance weighting is an exact interpolation method that ensures the estimated value of a point is influenced more by nearby points than by those farther away (Chang 2008). The general equation for an IDW algorithm is given by (Dodson and Marks 1997; Chang 2008):

$$z_0 = \frac{\sum_{i=1}^{s} z_i \frac{1}{{d_i}^k}}{\sum_{i=1}^{s} \frac{1}{{d_i}^k}} \qquad 1$$

Where z_0 is the estimated value at an unknown point, z_i is the known *z* value at point *i*, d_i is the Euclidean the distance between the ith point and point 0, *s* is number of know points and *k* is the specified IDW power. The power *k* controls the degree of local influence (Chang 2008). Dodson (1997) used a value of $k = 2$. An important characteristic of IDW algorithms is that the estimated points are bounded by the minimum and maximum values of the known points (Chang 2008).

2.2.2 Kriging

Kriging is a geostatistical spatial interpolation that is best known in the earth sciences (Myers 1993). Due to the statistical methods that are involved in the computation, this style of interpolation has the added advantage that it can provide some measure of the certainty or accuracy of the predictions (Environmental Systems Research Institute 2008). Kriging interpolation assumes that the distance between known points reflects a spatial correlation that be used to explain variation within the surface (Environmental Systems Research Institute 2008). It uses a semivariogram to measure the spatial correlated component.

There are many different variants of Kriging, however the three well known methods include: Simple, Ordinary and Universal. Simple Kriging assumes that the mean of the data set is known, which is typically unrealistic and inapplicable to most geophysical process (Chang 2008). It will not be discussed here. Universal Kriging assumes that the data has an overwhelming trend that can be modeled by a deterministic function (Environmental Systems Research Institute 2008). The process begins with the creation of a deterministic function which is subsequently subtracted from the known measured points after which the autocorrelation is modeled from the random errors. After the model is fit to the random errors, the deterministic function is added back to the predictor to give a useful result. Universal Kriging should only be used when you know there is a trend in the data, and one can provide a scientific justification to describe it (Environmental Systems Research Institute 2008). Ordinary Kriging is the most general and typically widely used variant (Environmental Systems Research Institute 2008) and assumes a constant, unknown mean. The general equation for estimating a value at a point z_o is given by (Chang 2008):

$$z_0 = \sum_{i=1}^{s} z_x W_x \qquad 2$$

Where z_x is the known value at point x, W_x is the weight associated with point x and s is the number of known points used in estimation. The weights W can be found from solving a system of linear equations of the form:

$$\begin{bmatrix} \gamma(h_{11}) & \dots & \gamma(h_{1s}) & 1 \\ \vdots & \ddots & \vdots & \vdots \\ \gamma(h_{s1}) & \dots & \gamma(h_{ss}) & 1 \\ 1 & \dots & 1 & 0 \end{bmatrix} \begin{bmatrix} W_1 \\ \vdots \\ W_s \\ \lambda \end{bmatrix} = \begin{bmatrix} \gamma(h_{10}) \\ \vdots \\ \gamma(h_{s0}) \\ 1 \end{bmatrix} \qquad 3$$

Where $\gamma(h_{ij})$ is the semivariance between known points i and j, $\gamma(h_{i0})$ is the semivariance between the ith known point and the point to be estimated and λ is a Lagrange multiplier which is added to ensure the minimum possible estimation error (Chang 2008). From this we can observe that Kriging takes into account the semivariances between estimated as well as known points. The function $\gamma(h_{ij})$ is found from computing an interpolate (non-exact) to the semivariogram. The most popular functions are spherical, exponential and linearly based. This interpolate is termed the semivariogram model.

The weights found in equation 3 obey:

$$\sum_{i=1}^{s} W_i = 1 \qquad 4$$

Variance estimates can be calculated by (Chang 2008):

$$s^2 = \left[\sum_{i=1}^{s} W_s \gamma(h_{s0})\right] + \lambda \qquad 5$$

There exists several less than desirable properties of Kriging when applied to a data set. Perhaps the most important is that in the spatial interpolation of temperature, relative humidity and other atmospheric variables, there is often an over-smoothing of the data (Myers 1993). However, Dodson (1997) concluded that this over smoothing wasn't as excessive as previously thought when applied to temperature variables in complex terrain. Secondly, the fact that Kriging is an inexact interpolate allows for values at meteorological stations to be different than what was measured. As there is very limited known data as is, there is therefore no reason to discard known values. In addition variables in a certain location may be heavily restricted to a certain range, as would be indicated by the known values. However, the inexact interpolate may add unrealistic noise to the modeled data, leading to incorrect results that are based on these data. Due to Kriging's statistical nature, a basic requirement is a large sampling of values with which to build the semi-variogram; failure to meet such a requirement would bring into question the accuracy of the semi-variogram and the subsequent interpolate. The typically low meteorological station density of a basin means that Kriging is not a proper choice for the domain over which one intends to interpolate. Due to the limited station density of the study site as well as the desire to preserve the measured values, Kriging will not be used in the simulations.

2.2.3 Thin-plate Spline with Tension

Thin plate splines are a surface interpolate that passes through all known points (exact interpolate) and has the least possible change in slope at all points (Chang 2008). Unlike the above mentioned IDW interpolation technique, the predicted values from a spline are not confined to the limits imposed by the maximum and minimum of the known values. Therefore, a common problem associated with splines is steep gradients (overshoots) in data poor areas. Methods to control these overshoots have been developed and are referred to as Radial Basis Functions (RBF). The class of RBFs is large with many variants such as regularized splines with tension (Mitasova and Mitas 1993) and the method used herein, thin-plate spline with tension. Thin plate spline with tension takes the form (Chang 2008):

$$z_0 = a + \sum_{i=1}^{n} A_i * R(d_i) \qquad 6$$

Where a is the trend function and $R(d_i)$ is the basis function:

$$R(d_i) = -\frac{1}{2\pi\varphi^2}\left[ln\left(\frac{d*\varphi}{2}\right) + c + K_0(d*\varphi)\right] \qquad 7$$

Where φ is the weight (taken to be 0.1), *d* is the Euclidian distance between the known and unknown points, *c* is Euler's constant taken to be 0.577215 and K_0 is the second type, modified Bessel function (typically referred to as BesselK). To solve equations 6 and 7, calculate *R(d)* for all the combinations of the known points and unknown point. These values for R can be inserted into equation 6, which can then be written in matrix form

$$Ax = b \qquad 8$$

Where A_i values are placed in *A* and *x* are the unknown weights and *b* are the known values.

$$x = \begin{bmatrix} a \\ A_1 \\ A_2 \\ \vdots \\ A_n \end{bmatrix} \qquad 9$$

3. ATMOSPHERIC VARIABLES

3.1 Air temperature

Air temperature can be interpolated spatially by a variety of schemes such as those discussed above, however these typically only work well over flat, homogenous terrain and break down when applied to complex terrain (Dodson and Marks 1997; Liston and Elder 2006) due to the effects of elevation on temperature. Therefore it is important to take into account the strong elevation-temperature relationships that are known to exists (Dodson and Marks 1997) when spatially interpolating air temperature. The simplest way of accounting for this relationship is via the lapse rate. As a parcel of air rises, it expands in volume and cools in temperature. If no heat is added or withdrawn from this parcel, it is said to be an adiabatic process (Wallace and Hobbs 2006). The change in the parcel's temperature as a function of height is termed the dry adiabatic lapse rate which has a value of $-9.81\ \frac{℃}{Km}$ (Wallace and Hobbs 2006). In reality however, air movement is typically not truly adiabatic as energy is added to/removed from the system via condensation and evaporation, radiation and mixing of air masses (Dodson and Marks 1997). The rate at which a parcel of air actually cools is termed the environmental lapse rate and a mean value of $-6.5\frac{℃}{km}$ (Dodson and Marks 1997) is normally used. Although such constant linear lapse rates are simple to employ, they do not always reflect the changes due to seasonal and spatial variability. Kunkel (1988) proposed variable, monthly based air temperature lapse rates as indicated in Table 1.

Table 1: Month lapse rates for North America (Kunkel 1988; Liston and Elder 2006)

Month	Air temperature Lapse Rate ($^{\circ C}/_{km}$)
January	4.4
February	5.9
March	7.1
April	7.8
May	8.1
June	8.2
July	8.1
August	8.1
September	7.7
October	6.8
November	5.5
December	4.7

Once a lapse rate has been established, the temperatures can be lowered to a common reference level (typically sea level, 0.0m) using these lapse rates (be it constant, measured or the monthly variable). Once at the common reference level they can be gridded via an interpolate using a method of choice. Once the spatial interpolation has been completed they are raised via the DEM and the lapse rate to account for elevation changes.

A constant lapse rate equation takes the form:

$$T_0 = T_{stn} - \Gamma(z_o - z_{stn}) \quad 10$$

Where T_0 is the reference temperature (°C), T_{stn} is the measured air temperature at a point (°C), Γ is the lapse rate (°C/Km), z_0 is the reference level (0.0 m for sea level) (m) and z_{stn} is the elevation of T_{stn} (m).

Dodson and Marks (1997; Marks 1990) proposed a method of lowering and raising air temperatures based on the potential temperature equation. This method assumes neutral atmospheric stability, however it should be noted that the atmosphere is typically not neutrally stable (Dodson and Marks 1997).

Potential temperature can be estimated from:

$$\Theta_a = T_z \left(\frac{P_0}{P_z}\right)^{\frac{R}{m c_p}} \quad 11$$

Where Θ_a is the sea-level potential temperature (K), T_z is the measured air temperature (K), P_0 is sea-level pressure ($\approx$ 1.0e5 Pa), P_z is the air pressure at elevation z (m), R is the gas constant (8.3143 $\frac{\mathrm{J}}{\mathrm{Mol\ K}}$), m is the molecular weight of dry air (0.02897 kg/mol) and c_p is the specific heat of dry air at a constant pressure (1005 $\frac{\mathrm{J}}{\mathrm{Kg\ K}}$). P_z can be derived using a form of the hydrostatic equation (Dodson and Marks 1997)

$$P_z = P_0 * \frac{T_b}{T_b + \Gamma z}^{\frac{mg}{\Gamma R}} \quad 12$$

Where T_b is an assumed sea level temperature (300 K), Γ is the lapse rate ($\mathrm{K/m}$; Dodson and Marks (1997) used a value of -0.0065 K/m), z is the station elevation (m) and g is the acceleration due to gravity (9.80616 $\frac{\mathrm{m}}{\mathrm{s}^2}$). Equations 10 and 11 can then be used, after spatial interpolation, to solve for the elevation corrected temperatures. As per the naming convention employed by Dodson and Marks (1997) the method employed by equation 6 is termed the *Linear Lapse Rate Adjustment* (LLRA) and the method in equation 11 is termed the *Neutral Stability Algorithm* (NSA).

This paper will apply the following to the research domain:

1. LLRA with monthly variant lapse rate (as per Table 1)
2. NSA with constant linear lapse rate following Dodson and Marks (1997)

In addition, two methods of spatial interpolation for each scheme are to be evaluated – an IDW (*k*=2) interpolate and a thin plate spline with tension method as described in the previous section.

3.2 Relative Humidity (RH)

Relative humidity (RH) is defined as (Wallace and Hobbs 2006):

$$RH \equiv 100\frac{w}{w_s} \simeq 100\ \frac{e}{e_s} \quad 13$$

Where w and w_s are actual and saturated mixing ratios with respect to a plane surface of water/ice and where e and e_s are the actual and saturated vapour pressures, respectively (Wallace and Hobbs 2006).

In order to spatially interpolate RH, it must be converted to a vapour pressure. This can be accomplished via the following:

Let e_s be the saturation vapour pressure (Pa). Then for a given temperature T (°C):

$$e_s = a\ \exp\left(\frac{bT}{c+T}\right) \quad 14$$

Where a, b, c are constants which vary for evaporation over water or ice as per Table 2 (Liston and Elder 2006).

Table 2: Constants for equation 10

Constant	Water	Ice
a	611.21 Pa	611.15 Pa
b	17.502	22.452
c	240.97℃	272.55℃

Equation 13 can then be solved for e.

Using the actual vapour pressure, *e*, the dewpoint temperature T_d(℃) can be calculated from (Liston and Elder 2006):

$$T_d = \frac{c \ln\left(\frac{e}{a}\right)}{b - \ln\left(\frac{e}{a}\right)} \quad 15$$

Following Kunkel (1988; Liston and Elder 2006) a dewpoint temperature lapse rate, Γ_d(℃/km), can be calculated via:

$$\Gamma_d = \lambda \frac{c}{b} \quad 16$$

Where λ (m^{-1}) is a vapour pressure coefficient as per Table 3 and the constants in equations 15 and 16 (*a*, *b*, *c*) are from Table 2.

Table 3: Vapour pressure coefficient (Kunkel 1988)

Month	Vapour pressure coefficient (km^{-1})
January	0.41
February	0.42
March	0.40
April	0.39
May	0.38
June	0.36
July	0.33
August	0.33
September	0.36
October	0.37
November	0.40
December	0.40

The dew point temperatures can be lowered to a common reference level (0.0m for sea level) using the dewpoint lapse rate as per equation 16. Once at a common reference level, the dewpoint temperatures are interpolated and then raised to the DEM height using the lapse rate as per equation 16. These dewpoint temperatures can then be converted to RH values via equations 13 and 14 by replacing T by T_d in equation 14.

This paper will apply the following to the research domain:

1. Distribute RH via an IDW scheme
2. Distribute RH via the thin plate spline with tension scheme

4. R A D I A T I O N

4.1 Introduction

Solar shortwave radiation provides a large source of energy to the Earth's surface and plays a principal role in most surface/climate processes, as well as providing the driving force for many other atmospheric, hydrological and biological processes (Ranzi and Rosso 1995; Oliphant et al. 2003). On a theoretical infinite flat plane, the incoming radiation incident at the ground is comprised of diffuse beam from the sky and direct beam from the sun. However, in an area of complex terrain there is a third component: diffuse and direct reflected from nearby terrain, as per Figure 1. As well, and most importantly, local topography can shade regions and the slope and aspect separate from shading can dramatically changing the energy budget of a location.

Figure 1: Diagram showing radiation in complex terrain.

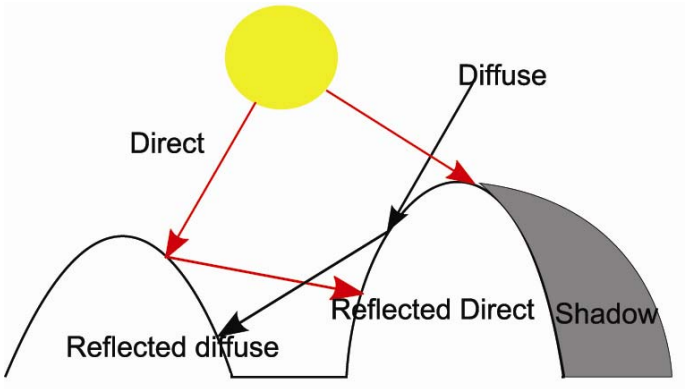

Variations in slope, aspect and local terrain heights can shadow surrounding terrain. This variability changes with time of day, time of year and latitude. This can create cycling where locations move in and

out of direction radiation and can create huge differences in local shortwave energy budgets and can play a principal role in, for example, melt patterns of glaciers nested in highly shaded cirques, microclimate, air and soil temperature regimes, evapotranspiration, soil moisture and photosynthesis and subsequent vegetation patterns. If the surrounding topography sufficiently is tall, such as in the Rocky Mountains, it can completely block locations from receiving any direct incoming solar radiation if the sun is low in the horizon, such as during the winter months.

The general, the driving equation of clear sky incoming solar radiation to a surface of a given slope and aspect was outlined by Garnier and Ohmura (1968). Using vectors representing the position of the sun with respect to a surface and transferring this local system into a global system to account for latitude and solar position, they derived the following equation for a time period of t_2-t_1.

$$I_d = I_o \int_{T_1}^{T_2} p^m * \cos(\boldsymbol{X} \cdot \boldsymbol{S})\, dT \qquad 17$$

Where

I_o is the solar constant

T_1 and T_2 is the period to solve for

p is the zenith mean path transmissivity of the atmosphere

m is the optical air mass as function of time H

The angle between the sun and the slope, given by $\cos(\boldsymbol{X} \cdot \boldsymbol{S})$, is:

$$\begin{aligned} \cos(\boldsymbol{X} \cdot \boldsymbol{S}) = [&(sin\phi cosH)(-cosA\ sinZ_x) - sinH\ (sinA\ sinZ_x) \\ &+ (cos\phi cosH)cosZ_x]cos\delta \\ &+ [cos\phi(cosA\ sinZ_x) + sin\phi cosZ_x] \end{aligned} \qquad 18$$

Where

ϕ is the latitude of the slope

H is the hour angle measured from solar noon, positively towards the west

A is the azimuth of the slope measured north through east

Z_x is the zenith angle of the X (slope) vector (see Garnier and Ohmura for full vector diagrams)

δ is the sun's declination, positive north of the equator, negative south of the equator

An approximation for the optical air mass, m, can be found from $m = secZ = \frac{1}{cosZ}$ where Z is the zenith angle of the sun. However, this approximation is only valid for $Z \leq 60^o$ due to the fact that $\lim_{Z \to 90} secZ = \infty$, implying an infinite air mass at the horizon, which is not valid. Therefore, although this approximate is convenient, for values of $Z \geq 60$ a look up table is needed, such as List (1968). Young (1994) developed the following equation for m, which he claims to have an error at the horizon of 0.0037 (note: air mass is unitless).

$$m = \frac{1.002432 * cos^2 Z + 0.148386 * cosZ + 0.0096467}{cos^3 Z + 0.149864 * cos^2 Z + 0.0102963 * cosZ + 0.000303978} \quad 19$$

Young noted that:

> *[…] the precision given in the coefficients in relation [40] is intended only to prevent round-off errors near the horizon; it does not indicate either the true accuracy of the formula or the precision of individual coefficients.*

However, for these equations to be fully valid, some measure of clear sky transmissivity is needed. If the sunshine ratio $\frac{n}{N}$ is available, where *n* is total sunshine hours and *N* is the maximum theoretical sunshine hours, an approximation can be obtained. In remote areas where maintenance of the sunshine records is not possible, this ratio may be impossible to reliably obtain as snow fall, organic matter, et cetera may obscure the recording device. As well, once clouds and other atmospheric particulate is taken into account, these equations begin to lose their ability to approximate direct incoming solar radiation as the diffuse component begins to grow as the direct component lessens. So although it is attractive and more realistic to take into account the shadowing effects of surrounding topography and upper atmospheric properties, it is sometimes difficult due to data constraints, including obtaining appropriate DEMs at a satisfactorily high resolution for the model domain (Ranzi and Rosso 1995) and high resolution driving data. In addition to the data constraints, high resolution grids require significantly more computing power, which may not be available. Therefore, if possible, it is attractive to model incoming solar radiation without these constraints in terms of computational simplicity, as well as a lack of necessary driving data.

Due to the constraints of a physically based equation, a relationship between transmissivity and some other easily measured variable is desirable such that a, hopefully, more valid approximation can be made. There have been many empirical relations between multiple combinations of temperature, relative humidity and precipitation such as that of Bristow and Campbell (1984; 1985), Weiss (2001), Thornton and Running (1999) and Thornton et al. (2000) to name but a few present in the literature. For a comparison of many of these types of models please see Evrendilek and Ertekin (2008). The largest downside of these types of equations is that they do not take into account terrain characteristics outside of their influence on the driving data. Therefore in complex terrain, there have been examples, such as Walter et al. (2005), of where these methods have worked well at point locations, but few, if any, providing examples of distributing them spatially to estimate incoming solar radiation at another location in the complex terrain.

Since there are serious data constraints on being using physics based transmittance models, quasi-physically based models such as Liston and Elder (2006) have been presented to address the problems of cloud cover through empirical relationships, while still accounting for terrain shading. Another option is to use the basic idea of Garnier and Ohmura (1968), but to take average estimated values for the transmittance and to separate the direct and diffuse beams using average values. The GIS software ArcGIS Desktop 9.3 includes such a method built in, called 'Solar Analyst', which allows for point and area daily solar radiation calculations. Although the variables can be calibrated to provide fantastic location-specific correlation, these calibrations require knowledge of the transmittance. However, if transmittance information was available, it may be more appropriate to use a different model such as that put forth by Oliphant (2003) that is more economical to run, yet is still physically based. Therefore, a tool such as Solar Analyst can provide values which require no atmospheric forcing data, allowing for its applicability to areas without meteorological stations.

The method of Oliphant is notable for breaking the isotropic and circumsolar diffuse into two components which they claim can significantly reduce errors – potentially up to 40%. Their method is briefly described below.

Extraterrestrial irradiance at the top of the atmosphere orthogonal to the atmosphere, K_{oh} (W/m^2), is defined as:

$$K_{oh} = \frac{I}{r^2} cosZ \qquad 20$$

Where I is the solar constant (Oliphant et al. used a value of ≈1356 W/m^2), r is the ratio of the earth-sun distance to its mean, and Z is the zenith angle which is the angle of the solar beam relative to the surface normal. Using Equation 20, incident direct (K_{sh}) and diffuse (K_D) radiations are given by:

$$K_{sh} = K_{oh} * \tau^m \qquad 21$$

$$K_D = (0.271 - 0.294 * \tau^m) * K_{oh} \qquad 22$$

Where τ is the atmospheric transmittance.

4.2 Flat plane, daily temperature based transmittance

The following provide a method of estimating incoming radiation using temperature to estimate transmittance. However, these do not take into account shading in complex terrain and are anticipated to overestimate radiation in locations which experience shadows throughout the day.

The radiation incident at a point on the Earth is given by (Walter et al. 2005):

$$S = T_t * S_o \qquad 23$$

Where T_t is the atmospheric transmittance and S_o is the maximum potential theoretical extraterrestrial solar radiation (kJ/m^2).

Campbell-Bristow-Walter (CBW)

The potential extraterrestrial solar radiation on a horizontal plane is taken to be:

$$S_o = \frac{S'}{\pi} * \{cos^{-1}(-tan\delta * tan\phi) * sin\phi * sin\delta + cos\phi * cos\delta * \sin[cos^{-1}(-tan\delta * tan\phi)]\} \quad 24$$

Where S' is taken as $117.5 * 10^3$ kJ m^{-2} day^{-1} (Garnier and Ohmura 1968; Walter et al. 2005), ϕ is the latitude of the location (radians) and δ is the solar declination (radians). Solar declination may be calculated in a variety of methods; however Walter et al. (2005) use a modified version of the method proposed by Rosenberg (1984):

$$\delta = \frac{23.5\,\pi}{180} * sin\left(\frac{2\pi}{365} * (J - 80)\right) \quad 25$$

Where J is the day number (Jan. 1 = 1, Jan. 2 = 2, etc). If $J = 1$, then the $J - 80$ term is taken as a negative value. One method of estimating the transmittance of the atmosphere, T_t, uses an equation derived by Bristow and Campbell (1985), and subsequently modified by Campbell (Walter et al. 2005):

$$T_T = 0.75 * \left[1 - \exp\left(-\frac{B}{S_{o30}} * (T_x - T_n)^2\right)\right] \quad 26$$

Where B is an empirical coefficient, S_{o30} is the potential extraterrestrial solar radiation 30 days previous to the simulation day (MJ m^{-2}) and T_x, T_n are the daily maximum and minimum temperatures respectively(℃) (Walter et al. 2005).

B is given as (Walter et al. 2005):

$$B = 0.282 * \phi^{-0.431} \quad 27$$

$$B = 0.170 * \phi^{-0.979} \quad 28$$

Where equation 27 is for summer and equation for 28 for the winter, where summer encompasses the 90 days preceding and 90 days following the summer solstice and winter is the rest of the year.

Annandale

Annandale (2002) suggested a method for calculating transmittance based on the square root of the daily minimum and maximum air temperatures and an elevation correction factor. With a slight deviation in calculation S_o than the method used by CBW, T_t can be calculated via (Annandale et al. 2002):

$$T_t = k_{Rs} * (1 + 2.7 * 10^{-5} * Alt) * \sqrt{T_{max} - T_{min}} \quad 29$$

Where k_{Rs} is an empirical constant with values of 0.16 and 0.19 for inland locations and coastal locations respectively, *Alt* is elevation (m), and T_{max} (℃), T_{min}(℃) are daily maximum and minimum air temperatures.

S_o $\left(\frac{MJ}{m^2 day}\right)$ is calculated by:

$$S_o = \frac{S^{'}D_{rel}}{\pi} * \{cos^{-1}(-tan\delta * tan\phi) * sin\phi * sin\delta + cos\phi * cos\delta * \sin[cos^{-1}(-tan\delta * tan\phi)]\} \quad 30$$

Where D_{rel} is the inverse relative distance between the earth and sun. DOY is the day of the year (Jan 1st = 1, Jan 2nd = 2, …).

$$D_{rel} = 1 + 0.033 * \cos\left(\frac{2\pi * DOY}{365}\right) \quad 31$$

$S^{'}$ is the solar constant $\left(118.08 \frac{MJ}{m^2 day}\right)$. Solar declination ($\delta$) (radians) is calculated as:

$$\delta = 0.409 * \sin\left(\frac{2\pi}{365} * DOY - 1.39\right) \quad 32$$

4.3 Shadowing, physically based

The following methods allow for shadowing (where topography blocks a slope) there is no incoming direct solar radiation and all radiative energy is from diffuse radiation.

Liston and Elder

Incoming solar short wave radiation, Q_{si} (W/m^2), incident to a slope with an angle between the slope and radiation take as *i*, is given by:

$$Q_{si} = S^* * (\psi_{dir} * \cos i + \psi_{dif} * \cos Z) \quad 33$$

Where S^* is the solar irradiance incident at the top of the atmosphere ($S^* = 1370$ W/m^2), and ψ_{dir} , ψ_{dif} are the direct and diffuse radiations respectively. Z is the solar zenith angle given by:

$$cosZ = sin\delta * sin\phi + cos\delta * cos\phi * cos\tau \quad 34$$

Where ϕ is latitude, δ is solar declination and τ is the hour angle measured from local solar noon.

$$\tau = \pi\left(\frac{h}{12} - 1\right) \quad 35$$

Where *h* is the hour of the day

$$\delta = \phi_T * cos\left[2\pi\left(\frac{d - d_r}{d_y}\right)\right] \quad 36$$

Where ϕ_T is the tropic of Cancer (23° 26′ 22″), d is day of the year, d_r is day of the summer solstice and d_y is the average number of days in a year (typically 365). The angle *cos i* is given by:

$$\cos i = \cos\beta * \cos Z + sin\beta * sinZ * \cos(\mu - \xi_s) \quad 37$$

Where β is the terrain slope angle given by:

$$\beta = arctan\left[\left(\frac{\partial z}{\partial x}\right)^2 + \left(\frac{\partial z}{\partial y}\right)^2\right]^{1/2} \quad 38$$

Where z (m) is height at a DEM cell and x (m) and y(m) are the Euclidian coordinate directions. The terrain slope azimuth, ξ_s, is given by:

$$\xi_s = \frac{\pi}{2} - tan^{-1}\left(\frac{\partial z/\partial y}{\partial z/\partial x}\right) \quad 39$$

Note that for this equation, south is defined as having zero azimuth.

The solar azimuth, μ, is given by:

$$\mu = sin^{-1}\left(\frac{cos\delta * sin\tau}{sinZ}\right) \quad 40$$

Using the equations from sections 3.1 and 3.2, temperature and RH can be elevated to the 700mb level of the atmosphere. From this, a cloud cover fraction,σ_c, can be defined as:

$$\sigma_c = 0.832 * exp\left(\frac{RH_{700} - 100}{41.6}\right) \quad 41$$

The cloud cover fraction obeys $0 \leq \sigma_c \leq 1$.

The results of this can be combined into an equation for diffuse and direct beam radiations, taking into account atmospheric scatter, absorption and cloud cover using the direct and diffuse components given by:

$$\psi_{dir} = (0.6 - 0.2 * cosZ)(1.0 - \sigma_c) \quad 42$$

$$\psi_{dif} = (0.3 - 0.1 * cosZ)\sigma_c \quad 43$$

ArcGIS Solar Analyst

ArcGis by Environmental Systems Research Institute, Inc. (ESRI) provides, arguably, an industry standard GIS product. Through the Spatial Analyst toolkit add on to the ArcGis 9.3 product, solar radiation calculations can be performed for an area. A notable feature of this method is that no atmospheric data is required. It utilizes default (although configurable) variables, such as transmittance, to calculate incoming solar radiation. Because knowledge of the atmosphere is required for calibration, which if known, other methods might be better suited, the values were left as default in order to simulate a situation where very little about the site is known, such as in preparation for a land use study or as a preliminary step to place meteorological stations is areas such that basin highs and lows could be covered. Parameters utilized are:

Sky Size = 200

Days = 1-366 (2008 is a leap year)

Hour interval = 1

Hour interval = 0.5

Everything else was default

A full method description is provided in the ArcGis 9.3 documentation and online through ESRI support[1]; a brief outline will be given below.

For every point of interest three steps must be performed:

1. Calculation of an upward looking hemispherical viewshed, based on topography
2. Overlay of the viewshed on a direct sunmap to calculate an estimated direct radiation.
3. Overlay of the viewshed on a diffuse sky map to calculate an estimated diffuse radiation

Viewshed calculations follow the algorithm developed by Rich, et al.(1994) and Fu and Rich (2002). Total incoming solar radiation (W/m^2) is:

$$Qsi_{tot} = Dir_{tot} + Dif_{tot} \quad 44$$

Total direct insolation, Dir_{tot}, from the sunmap sector, $Dir_{\theta,\alpha}$, is

$$Dir_{tot} = \sum Dir_{\theta,\alpha} \quad 45$$

The direct insolation from the sunmap sector with a centroid at zenith (θ) and azimuth angle (α) is

$$Dir_{\theta,\alpha} = I_0 * \beta^{m(\theta)} * SunDur_{\theta,\alpha} * SunGap_{\theta,\alpha} * \cos\left(AngIn_{\theta,\alpha}\right) \quad 46$$

Where

I_0 is the solar flux incident to the top of the atmosphere, taken as 1367 W/m^2.

β is the transmissivity of the atmosphere, average over all wavelengths.

$m(\theta)$ is the relative optical path length.

$SunDur_{\theta,\alpha}$ is the time duration represented by the sky sector.

$SunGap_{\theta,\alpha}$ is the gap fraction for the sunmap sector.

$AngIn_{\theta,\alpha}$ is the angle of incidence between the centroid of the sky sector and the axis normal to the surface.

Relative optical length can found via:

$$m(\theta) = \frac{\exp\left(-0.000118 * elev - 1.638 * 10^{-9} * elev^2\right)}{\cos\left(\theta\right)} \quad 47$$

Where

θ is the solar zenith angle

elev is the elevation above sea level (m)

Surface orientation is accounted by:

[1] http://webhelp.esri.com/arcgisdesktop/9.2/index.cfm?TopicName=Solar_radiation_analysis_equations

$$AngIn_{\theta,\alpha} = \text{acos}\,(\cos(\theta) * \cos(G_z) + \sin(\theta) * \sin(G_z) * \cos\,(\alpha - G_a)) \quad 48$$

Where

G_z is the surface zenith angle.

G_a is the surface azimuth angle.

The diffuse component can be found for each sky sector by:

$$Difn_{\theta,\alpha} = R_{glb} * P_{dif} * Dur * SkyGap_{\theta,\alpha} * Weight_{\theta,\alpha} * \cos\,(AngIn_{\theta,\alpha}) \quad 49$$

Where

R_{glb} is global normal radiation

P_{dif} is the proportion of global normal radiation flux that is diffused. 0.2 for very clear sky and 0.7 for very cloudy.

Dur is the time interval.

$SkyGap_{\theta,\alpha}$ is the gap fraction

$Weight_{\theta,\alpha}$ is the proportion of diffuse radiation originating in a given sky sector relative to all sectors.

$AngIn_{\theta,\alpha}$ as per equation 42.

The global normal radiation is found via:

$$R_{glb} = \frac{I_0 * \sum \beta^{m(\theta)}}{1 - P_{dif}} \quad 50$$

ArcGis allows for two sky types: uniform and overcast.

Uniform weights:

$$Weight_{\theta,\alpha} = \frac{cos\theta_2 - cos\theta_1}{Div_{azi}} \quad 51$$

Where

Θ_1 and θ_2 are the bounding zenith angles of the sky sector

Div_{azi} is the number of azimuthal division in the skymap

For the overcast sky, the weights are

$$Weight_{\theta,\alpha} = \frac{2 * cos\theta_2 + cos(2 * \theta_2) - 2 * cos\theta_1 - \cos\,(2 * \theta_1)}{4 * Div_{azi}} \quad 52$$

Total diffuse is thenL

$$Dif_{tot} = \sum Dif_{\theta,\alpha} \quad 53$$

5. MODEL DEVELOPMENT

In order to test these various methods and their applicability to complex terrain a computer model was created. The model was coded in object orientated C++ with a strong emphasis on modularity to allow for quick iteration of method combinations as well as focusing on parallelization. The parallelization aspect was handled through the Intel Threading Building Block Library[2]. The following section will describe model design considerations.

5.1 Design goals

The primary design goal of this project was to develop a model that allowed for extreme flexibility when loading datasets and during model creation. Given the nature of the project, multiple scenarios had to be considered; for example temperature interpolation with LLRA, NSA, Spline and IDW. Having hardcoded functions for each permutation would lead to coding overhead as well as large possibilities for logic error. An option was to write the low level functions in a high performance language such as C or C++ and then expose them to a higher level language such as Python which could act as a scripting language to allow for quick iteration. However, due to the interpreted nature of a language such as Python, there can be significant overhead. Given the large number of files to be processed, there was a worry that the overhead would decrease the model's performance to a level that would be detrimental and offset the advantages of the quick iteration and modularity as well as the parallelization. Therefore an alternative method was utilized. It involves breaking each process, be it interpolation of temperature, interpolation of RH, a Qsi method, et cetera into a module which does not maintain a state between calls. It does, however, have access to a large global variable pool where it can retrieve values and place values. Each module would then be called in a sequence defined in a configuration file for each time step present in the meteorological driving data. Figure 2 outlines the overall runtime architecture.

[2] http://www.threadingbuildingblocks.org/

Figure 2. Model execution

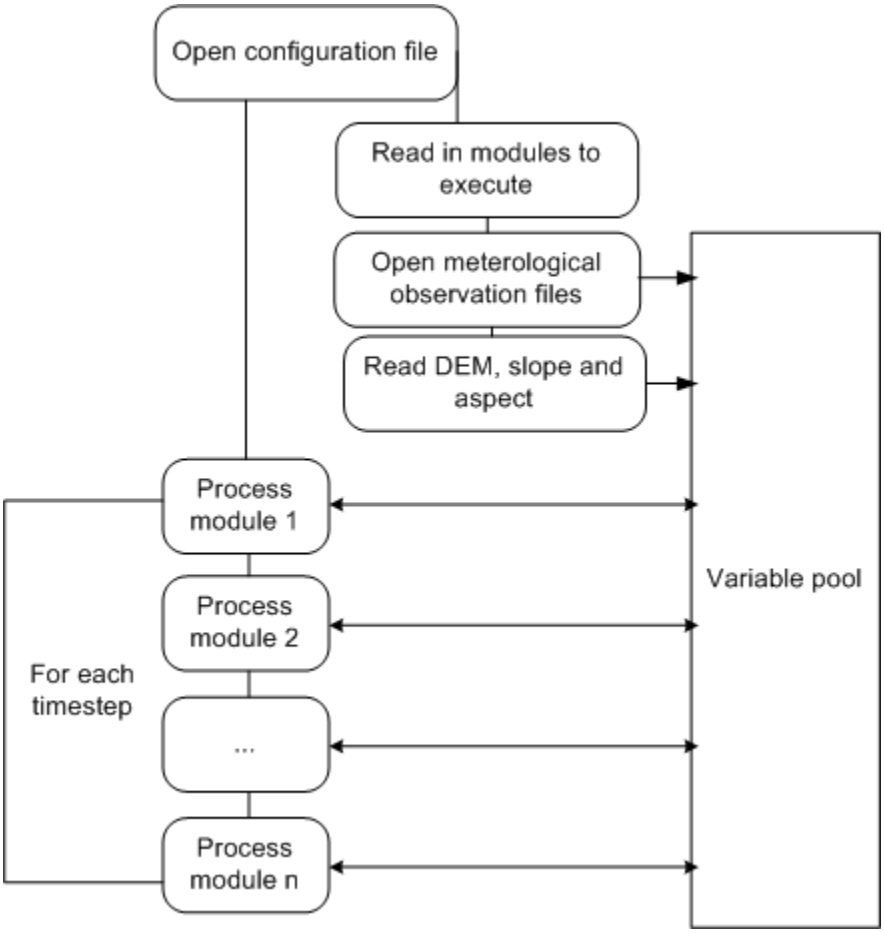

Figure 3. Sample configuration file

```
model:
{
    domain:
    {
        dem = "10m_dem.asc";
        slope   = "10m_slope.asc";
        aspect  = "10m_aspect.asc";
    };

    obs =
        (
            { stationID = "VistaView";
              file = "vv_15min.txt";
              easting = 628332 ;
              northing = 5648184;
              elevation = 1956.0;
            }
        );

    modules =
        (
        // Variable LLRA Temp min/max
            {
               name = "am_TempInterp";
               in = ("dem", "Tair", "Date", "IDW", "LLRA_var");
               out = ("TairLLRA");
            },
        // Qsi
            {
               name = "am_RHInterp";
               in   = ("dem","TairLLRA","Rh","Tair","Date","IDW","3000.0"); //3000m is taken to be 700 mb level
               out  = ("RH700_LLRA");
            }
            {
               name = "am_QsiListon";
               in = ("dem","slope","aspect","RH700_LLRA","Date");
               out = ("Liston_Qsi_LLRA");
            }
        //-------------------------------------------------------
        // Output
            {
               name = "am_RasterToFile";
               in = ("Liston_Qsi_LLRA","Date");
               out = ("Liston_Qsi_LLRA.asc");
            }
        );
};
```

As shown in Figure 3, the configuration file has a very familiar C feel to it. It is easy to edit, which allows for quick changes to be made to the model run in order to try different permutations. As well, for each change that occurred, a re-compile was not needed, which also decreased the iteration time.

5.2 Parallelization

With gridded models such as those implemented for this project, performance is a critical aspect and a serious bottleneck for model iteration. However, many aspects of gridded computer simulations

lend themselves very naturally to parallelization and this was exploited. Most notably, for all the processes examined herein, each grid cell's evaluation was independent of any other grid cells. Therefore a natural performance gain was easily obtained merely by parallelizing the iterations over the model domain. From this simple optimization, a fourfold speed increase was obtained.

5.3 Computer specifications and runtime

The models were run on an Intel Core2Quad Q6600 running at 3.2 GHz with 8 GB of ram. Although dependent upon the other tasks being run, the following list emphasis the downside of running high resolution models. The model memory footprint was about 30mb.

Method: CBW/ANA – **Interpolation**: IDW – **Time Step**: Daily **- Total Time ≈ 20 minutes**

Method: CBW/ANA – **Interpolation**: Spline – **Time Step**: Daily **- Total Time ≈ 3 hours**

Method: Liston – **Interpolation**: IDW – **Time Step**: Daily **- Total Time ≈ 5-6 hours**

Method: Liston – **Interpolation**: Spline – **Time Step**: Daily **- Total Time ≈ 15 hours**

If grids, instead of point values, are saved each step, hours are added to the run time, depending on disc access time. For 15min time steps, about 100 GB of data is generated per run.

The ArcGIS Solar Analyst is not included in the above list as its runtime is very different depending upon the parameters used. However, using a default value of 200 for the sky view resolution, a full grid takes about 5 minutes. If a larger value, such as 2800 to 4000 is used (which the ArcGIS documentation suggests for high resolution time periods of less than one day), computations can take upwards of an hour for a single timestep making them not very economic for quick iterative modeling.

6. D A T A & D O M A I N

6.1 Research Location

The model domain for this project is the Marmot Creek research basin operated by the Centre for Hydrology, University of Saskatchewan. It is located in the Kananaskis Valley, Alberta, Canada. The basin ranges in elevation from approximately 1450 to 2886 m.a.s.l and is located at 50^{o}58'N and 115^{o}W. Vegetation is characterized by a combination of clear cut, meadow, alpine and subalpine terrain. Figure 4 shows the model domain represented by a 10m DEM (derived from a 1m LiDAR DEM) with a 1m resolution airphoto overlain. Contours are every 100m. Meteorological stations used in the study are labeled.

Figure 4. Model domain. Ski runs from the Nakiska Mtn. ski area area visible in the southern portions of the domain.

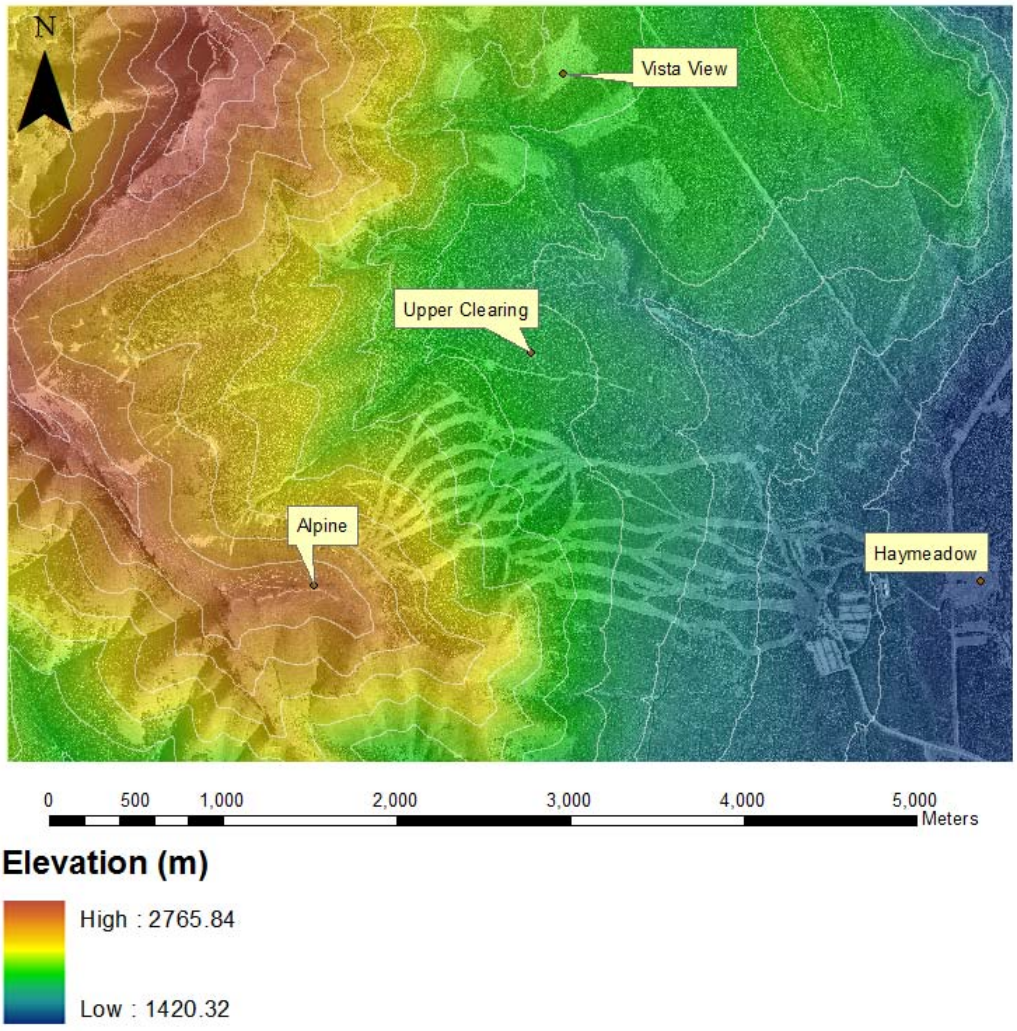

6.2 Data

The data used to drive this model was collected by the Centre for Hydrology at the University Of Saskatchewan. Variables utilized were air temperature, relative humidity and a LiDAR DEM collected at 1m spatial resolution, subsequently resampled to 10m using ArcGis 9.3 Spatial Analyst. Table 4 outlines the data resolution for each model.

Table 4: Model resolution

Process	**Data Resolution**
Campbell-Bristow-Walter (CBW)	15min averaged to daily
Annandale (ANA)	15min averaged to daily
Liston	15min, 10m DEM from resampled 1m LiDAR DEM
ArcGis Solar Analyst	10m DEM derived from resampled 1m LiDAR DEM

Days that contained more than 45min (3 time steps) of missing or bad data were removed; otherwise missing values were filled using a running mean. A total of 35 days were removed over the course of the simulation period which ran from January 1, 2008 to December 31, 2008. The incoming solar radiation measurements during the winter were most likely underestimated due to snow accumulation on the sensors (these are essentially unmanned stations); however the only correction to the incoming solar radiation was to correct all values less than 0 to be equal to 0.

In the following sections the following acronyms are used to denote stations:

VV - Vista View

HM - Haymeadow

NR - Nakiska Ridge (also called Alpine)

UC - Upper Clearing

While multiple stations are available in this area, many are very close to each other. However, the purpose of this study was to examine the applicability of distribution point data over a basin and points that are very close together typically don't have a large effect on the resulting overall interpolate. Due to the extra processing required for very small gain, only the above mentioned four points were chosen. However there were some issues with the incoming solar radiation measurements. Vista View does not have shortwave in, and Haymeadow had data quality problems for three-quarters of the year and had to be dropped from the cross validation. Therefore air temperature and relative humidity were used from all locations; however incoming shortwave comparisons were limited to Nakiska Ridge and Upper Clearing.

6.3 Cross Validation

In order to evaluate the effectiveness of the spatial interpolates and model, cross-validation was used. Cross validation compares the method by repeating the following for each known point in the set of known values (Chang 2008):

1. Remove a known point x_{ij} from the know-value set.
2. Use the interpolation scheme to estimate a value $x_{ij}{}^{*}$ for the previously removed point.
3. Calculate the error between x_{ij} and $x_{ij}{}^{*}$.

Error estimates were computed via Root Mean Square Error (RMSE) :

$$RMSE = \sqrt{\frac{1}{n}\sum_{i=1}^{n}(x_{io} - x_{im)}{}^{2}} \qquad 54$$

Where *o* denotes observed values and *m* are the modeled values. In addition the Nash-Sutcliffe (N-S) efficiency coefficient was calculated, which is found via (Nash and Sutcliffe 1970):

$$E = 1 - \frac{\sum_{i=1}^{n}\left(Qsi_o^i - Qsi_m^i\right)^2}{\sum_{i=1}^{n}\left(Qsi_o^i - \overline{Qsi_o}\right)} \qquad 55$$

Where

Qsi_o^i is the i[th] observed incoming shortwave value

Qsi_m^i is the i[th] modeled incoming shortwave value

$\overline{Qsi_o}$ is the mean observed incoming shortwave value

The efficiency E, has the range $(-\infty, 1]$. An efficiency of 1 indicates a perfect match of modeled Qsi with the observed data and an efficiency of 0 indicates that the model predictions are as accurate as the mean of the observed data. If E is within the range $(-\infty < E < 0)$, the observed mean is a better predictor than the model. The closer E is to 1, the more accurate the model. The R^2 was also calculated for the regression of Observed vs Model.

7. R E S U L T S

Of the four meteorological sites, three had shortwave radiation measurements – Haymeadow, Nakiska Ridge (Alpine) and Upper Clearing. The following two tables (5 and 6) show the cross validation results for each temperature and Qsi method (NSA with a constant lapse rate and LLRA with a variable, monthly lapse rate) as well as for each interpolation scheme. Legend for the header is

Interp = Interpolation Method

N-S = Nash-Sutcliffe efficiency coefficient

RMSE = Root mean square error

Stdev = Standard deviation

Temperature and relative humidity at the 15 minute interval is shown in table 6

Table 5. Comparison of modeled air temperature (Tair) and relative humidity (RH) versus the measured values. All mean, min, max etc are for the modeled values. Humidity is percent and air temperature is ^{o}C.

Var	Interp	Site	Lapse Rate	R^2	N-S	RMSE	Mean	Min	Max	Stdev
Tair	IDW	HM	LLRA	0.8950	0.8745	3.7103	3.35	-31.74	30.77	10.14
Tair	Spline	HM	LLRA	0.8835	0.8596	3.9235	3.46	-31.60	30.62	10.11
Tair	IDW	HM	NSA	0.8990	0.7923	4.7700	5.28	-29.08	32.43	9.78
Tair	Spline	HM	NSA	0.8872	0.7656	5.0696	5.51	-28.75	32.37	9.73
Tair	IDW	NR	LLRA	0.8809	0.8608	3.4351	-4.20	-36.81	22.53	9.35
Tair	Spline	NR	LLRA	0.8674	0.8442	3.6343	-4.28	-36.66	22.27	9.34
Tair	IDW	NR	NSA	0.8890	0.8482	3.5874	-4.64	-38.22	22.51	4.64
Tair	Spline	NR	NSA	0.8781	0.8281	3.8181	-4.84	-38.27	22.15	9.73
Tair	IDW	UC	LLRA	0.9758	0.9706	1.7043	0.69	-33.09	26.81	9.66
Tair	Spline	UC	LLRA	0.9806	0.9774	1.4947	0.52	-33.09	26.81	9.64
Tair	IDW	UC	NSA	0.9750	0.9366	2.5018	1.92	-31.75	27.97	9.55
Tair	Spline	UC	NSA	0.9799	0.9526	2.1637	1.61	-31.86	27.85	9.57
Tair	IDW	VV	LLRA	0.9857	0.9798	1.3770	-0.68	-34.20	26.67	9.71
Tair	Spline	VV	LLRA	0.9826	0.9761	1.4961	-0.71	-33.87	26.29	9.65
Tair	IDW	VV	NSA	0.9859	0.9855	1.1674	-0.07	-33.75	27.36	9.71
Tair	Spline	VV	NSA	0.9830	0.9825	1.2801	-0.12	-33.44	26.97	9.71
RH	IDW	HM	LLRA	0.6362	-0.5732	25.231	89.67	26.49	100.0	16.53
RH	Spline	HM	LLRA	0.4491	-1.2653	30.277	93.90	28.72	100.0	13.20
RH	IDW	HM	NSA	0.4583	-1.2795	30.371	94.07	28.75	100.0	13.01
RH	Spline	HM	NSA	0.5093	-0.9898	28.376	92.18	26.66	100.0	14.85
RH	IDW	NR	LLRA	0.1679	-2.4739	35.436	98.36	43.29	100.0	6.78
RH	Spline	NR	LLRA	0.1802	-2.4278	35.200	98.17	40.92	100.0	7.22
RH	IDW	NR	NSA	0.1609	-2.4927	35.532	98.43	43.97	100.0	6.59
RH	Spline	NR	NSA	0.1687	-2.4623	35.380	98.30	41.87	100.0	6.91
RH	IDW	UC	LLRA	0.4212	-0.8157	30.977	89.67	26.49	100.0	16.53
RH	Spline	UC	LLRA	0.3903	-0.8276	31.078	89.42	25.97	100.0	16.73
RH	IDW	UC	NSA	0.5086	-0.3625	26.834	85.50	23.74	100.0	18.58
RH	Spline	UC	NSA	0.4755	-0.3550	26.761	84.89	23.13	100.0	18.84
RH	IDW	VV	LLRA	0.3669	-2.0529	36.748	96.10	35.82	100.0	10.50
RH	Spline	VV	LLRA	0.3746	-2.0255	36.583	95.97	34.28	100.0	10.68
RH	IDW	VV	NSA	0.4066	-1.9126	35.894	95.43	34.38	100.0	11.35
RH	Spline	VV	NSA	0.4115	-1.8906	35.758	95.31	32.94	100.0	11.53

Due to the fact that the radiation models are driven primarily by the interpolated values, any errors or differences present should be reflected in the shortwave radiation results. Therefore it is important to examine the model accuracy (shown in Table 5) and consider if the different lapse rate methods have any effect. Two assumptions are made depending on which method is used: constant lapse rate over the basin (LLRA and NSA) and neutral atmospheric stability (NSA). If either of these assumptions is violated, it will have a detrimental effect on the modeled radiation values. Since there are more meteorological sites that can be used for validation for air temperature and relative humidity than for incoming shortwave radiation, when one examines the results for the distributed shortwave, if the spatially distributed driving data is correct and the model is shown to work at cross validation locations, there is a higher probability that the model is correct in the locations that lack verification observations.

One of the advantages of using spline interpolation, especially with temperature and RH is that the interpolated values are not constrained by the range of the known points. However that limitation does not seem to create much of a difference at any of the validation sites. Air temperature differences between the spline and IDW methods for a given lapse rate method are about $\pm 1^{o}C$; not a very large difference. The largest difference between the min and max and mean results stems from the differences in NSA and LLRA lapse rate methods. Generally the LLRA method is the strongest predictor due to the turbulent and non-stable atmospheric conditions present over a mountain range. Locations such as Nakiska Ridge which are locations of large atmospheric turbulence due to orographic lift and other associated atmospheric instabilities violate the assumption of a neutral atmosphere resulting in poorer prediction strength. The interpolation method used does somewhat effect the results with spline either worse than or as good as IDW, which is counter intuitive. The explanatory hypothesis is that the radial basis function used to control the overshoots of the spline interpolate is over smoothing the data, decreasing the spatial variability of the variables. There are many values that can be used as the tension weight; 0.1 was used as it is a common value in the literature as well as being a standard default value in many GIS tools such as ArcGIS. However in locations of such spatial variability there may be a benefit to using a higher/lower value. Further work would have to examine just how large of a difference the radial basis functions and tension value affect the over-smoothness in such highly spatially variable locations. One benefit of the spline interpolate not reflected in the numeric values presented above is that the wells typically associated with the IDW method are significantly decreased. Therefore artificially high/low values near to the control points is greatly reduced, increasing the applicability of the radiation maps generated. Relative humidity is surprisingly inaccurate. Frequently it estimates large portions of the grid to be 100% and overall, it significantly over estimates. Although no method is clearly better, LLRA and IDW generally do the best. Much like temperature, RH values that are interpolated via spline seem to smooth out, however the wells that are present in the IDW are not present when interpolated via spline. Table 6 below

highlights the model results for the cross validation sites. Unfortunately due to the data problems for the model year, only two sites were utilized for incoming shortwave radiation comparison – Nakiska Ridge and Upper Clearing. However both sites have significantly different elevations and terrain cover, so their cross validation is still very important.

Table 6: Cross-validation of incoming shortwave radiation. All units are W/m^2. Daily values are averages.

Model	Time Step	Interp	Site	Lapse rate	R^2	N-S	RMSE	Mean	Min	Max	Stdev
Liston	15 min	IDW	NR	NSA	0.7099	0.6032	137.941	96.86	0.00	444.05	127.13
Liston	15 min	IDW	NR	LLRA	0.6622	0.5999	138.524	97.28	0.00	444.03	127.06
Liston	15 min	Spline	NR	NSA	0.7114	0.6041	137.791	96.76	0.00	444.32	127.14
Liston	15 min	Spline	NR	LLRA	0.7046	0.6008	138.378	97.37	0.00	444.40	127.26
Liston	15 min	IDW	UC	NSA	0.6428	0.6253	128.520	110.41	0.00	467.15	141.07
Liston	15 min	IDW	UC	LLRA	0.6555	0.6320	127.350	108.02	0.00	465.97	138.75
Liston	15 min	Spline	UC	NSA	0.6456	0.6272	128.193	110.08	0.00	467.16	140.78
Liston	15 min	Spline	UC	LLRA	0.6576	0.6335	127.097	107.89	0.00	466.1	138.63
CBW	Daily	IDW	NR	-	0.7393	0.9986	51.186	117.58	11.59	305.92	69.70
CBW	Daily	Spline	NR	-	0.7471	0.9987	48.982	120.94	13.69	315.47	71.77
CBW	Daily	IDW	UC	-	0.5725	0.9966	64.747	96.14	8.45	257.06	53.29
CBW	Daily	Spline	UC	-	0.6117	0.9970	60.702	100.85	9.88	271.91	56.61
ANA	Daily	IDW	NR	-	0.8412	0.9992	38.330	150.44	26.83	359.83	91.09
ANA	Daily	Spline	NR	-	0.8445	0.9992	38.935	152.66	27.00	367.751	92.30
ANA	Daily	IDW	UC	-	0.7778	0.9981	48.382	135.35	25.06	321.27	79.03
ANA	Daily	Spline	UC	-	0.7856	0.9981	48.924	138.06	25.33	330.54	81.10
Liston	Daily	IDW	NR	NSA	0.8260	0.4920	63.737	96.86	26.11	200.51	52.24
Liston	Daily	IDW	NR	LLRA	0.8271	0.4884	63.967	97.27	29.53	200.30	51.06
Liston	Daily	Spline	NR	NSA	0.8259	0.4900	63.865	96.75	25.87	199.94	52.13
Liston	Daily	Spline	NR	LLRA	0.8263	0.4880	63.991	97.36	29.67	199.78	50.94
Liston	Daily	IDW	UC	NSA	0.7592	0.6902	50.779	110.40	32.60	209.22	56.23
Liston	Daily	IDW	UC	LLRA	0.7786	0.6977	50.164	108.02	28.93	208.41	55.74
Liston	Daily	Spline	UC	NSA	0.7611	0.6907	50.743	110.07	32.30	208.81	56.05
Liston	Daily	Spline	UC	LLRA	0.7809	0.6972	50.205	107.88	29.15	208.02	55.51
ArcGIS	Daily	-	NR	-	0.5995	0.5283	61.368	124.66	8.66	298.30	87.68
ArcGIS	Daily	-	UC	-	0.5525	0.5297	63.013	112.71	7.12	275.75	82.21

The 15 minute Liston and Elder model results showed minor sensitivity to the differences in the NSA and LLRA air temperature lapse rate methods. Generally however, the LLRA method produced better results. Due to the reliance on RH at the 700mb level which depends on a good temperature value, it follows that since the NSA method's assumptions are typically violated in areas of atmospheric instability such as the ridge (Nakiska Ridge); therefore LLRA produced a better RH value resulting in a better cloud fraction prediction. The interpolation method has no significant impact on the modeled insolation values aside from the reduction in artificial wells that are sometimes present with the IDW interpolation method.

With respect to the Campbell-Bristow-Walter and Annandale daily average values, these methods produced very good results in locations that are not heavily influence by topographic shading; however in locations that fall into shadow such as Upper Clearing, the results are not very strong. Although there is a high N-S value for all, the R^2 and RMSE show that the modeled values are affected by an over prediction in the shaded and slope regions. Generally these two methods provide good prediction. A larger study involving significantly more locations to test the sensitivity to shading would be required to conclusively show that the differences in the shaded regions can be accounted for by the difference in minimum and maximum air temperature. Annandale's method is able to better predict the insolation than the Campbell-Bristow-Walter method. Due to the inclusion of the altitude term, it is thought that this provides more applicability for use in higher elevation areas such as the Rocky Mountains. Spline interpolation is a better interpolation method, again presumably due to the ability to account for values not bounded by the known maxima and minima.

The 15 minute data from the Liston and Elder model was averaged into daily values and then compared to the observed values. Although it has strong R^2 values, the N-S values as well as the minimum and maximum values show that it fails to properly take into account the low winter daily values. Much like the 15 minute data, the resampled data is better with the LLRA lapse rate which is to be expected given the averaging of the 15 minute data. The inclusion of the shading and terrain slope does allow for more correct incoming shortwave radiation values, which can greatly impact the daily energy regime. Generally, this model performs quite well.

The daily values produced using the terrain based ArcGIS Solar Analyst show that some knowledge of location specific atmospheric variables is needed in order to produce meaningful results; at least in complex terrain. However, this was to be expected and the fact it does so well using average values and no knowledge of the meteorological conditions is encouraging and surprising. Such a method combined with some of the quasi-physically based methods described thus far could be a very strong candidate for use in complex terrain where terrain shading and limited viewsheds can create highly variable incoming shortwave radiation. However once problem with this method is that there is a strange

artifact present in the modeled data. Around day 170 there is a sharp valley which then immediately returns to an "expected" value. This is show in figure 5. Figure 5 shows the modeled NR and UC and measured NR and UC Qsi values.

Figure 5. ArcGIS Solar Analyst and measured incoming solar radiation. Note the sudden decrease in Qsi around day 150.

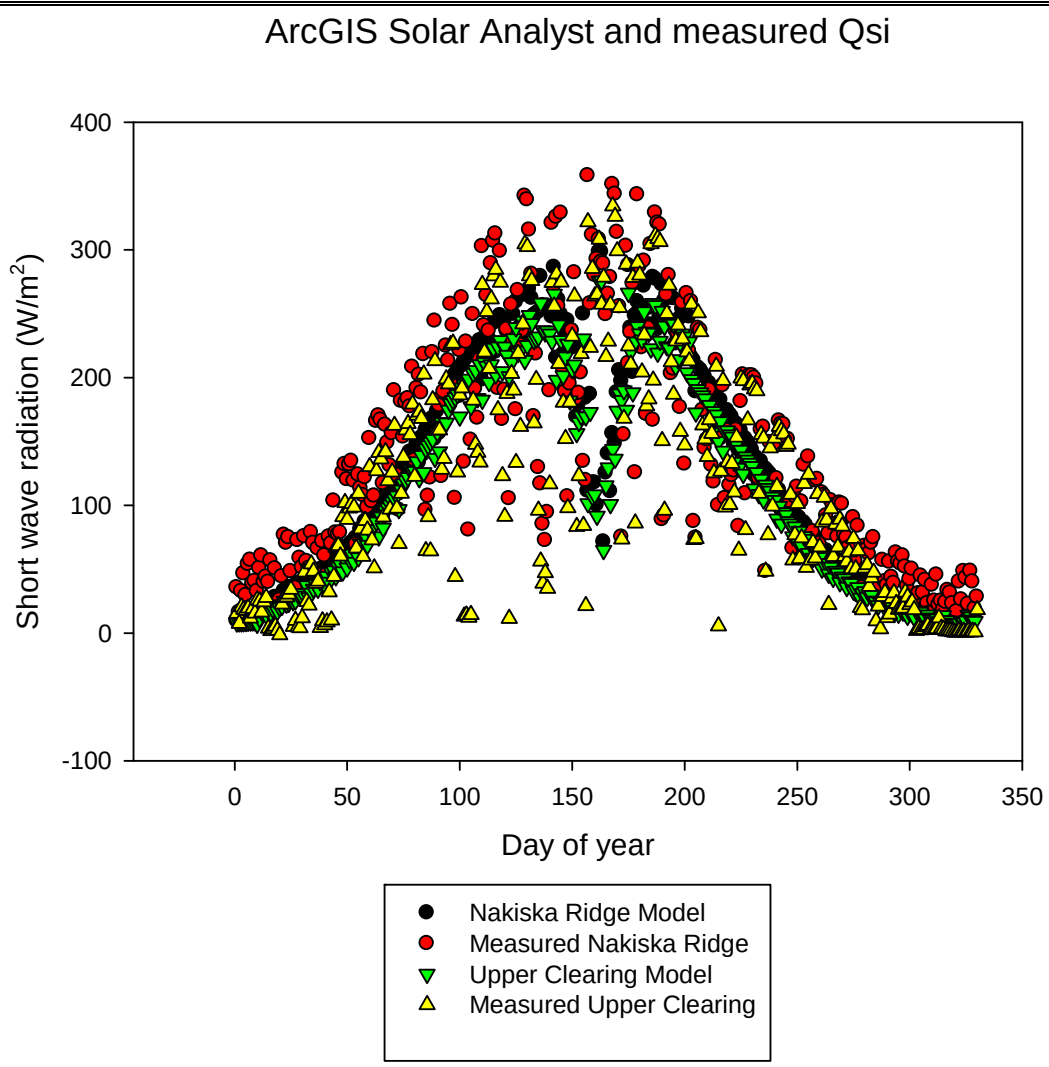

It is unclear why this artifact occurs, and it will be investigated further. One possibility is an artifact in the DEM may have contributed to the unexpected values as this method is completely driven using the DEM. However the DEM is not known to have produced unexpected values in the other simulations and the Solar Analyst tool was rerun with a DEM that is believed to be free of topographic artifacts. As a result, it is suspected that the DEM is not responsible for the artifact in Qsi in Figure 5.

A few select examples will be presented below showing the spatial variability in radiation and temperature over the domain as well as the effect of season on Qsi. The dates shown are January 1st , 2008 at 14:00 and July 1st , 2008 at 14:00. Only spline interpolation is shown for Liston due to the negligible spatial variations in the result (the images need to be much larger to see the differences) and LLRA lapse rate is used due to its typically stronger performance. For the daily methods, spline versus IDW will be shown.

Figure 7 shows the incoming shortwave as solved by Liston and Elder for January 1st, 2008. Extreme shading is visible along the ridge and this shows the importance of taking into account the shading. In Figures 7 and 8 the higher insolation value in the valley is counter intuitive. The reason for this is threefold. First, the ridges which compromise most of the higher elevations, are mostly north facing resulting in local shading and less exposure to the sun throughout the course of the day. Secondly, the topographic features to the east and south-east are not represented in the model domains DEM. Therefore the valley receives an insolation value which is significantly higher than in reality due to a lack of shading from outside the model domain. Thirdly, cloud formation typically favours ridge locations for development (Oliphant et al. 2003). Therefore there is a very good chance that these locations are typically cloudy resulting in decreased incoming shortwave radiation values. This cloud cover would affect the air temperature and the RH extrapolation to the 700mb level, resulting in a higher cloud cover fraction, which would result in a lower insolation value.

Figure 7: Liston model with the LLRA lapse rate utilizing Spline interpolation; Date : Jan 01, 2008 14:00; Units = W/m^2

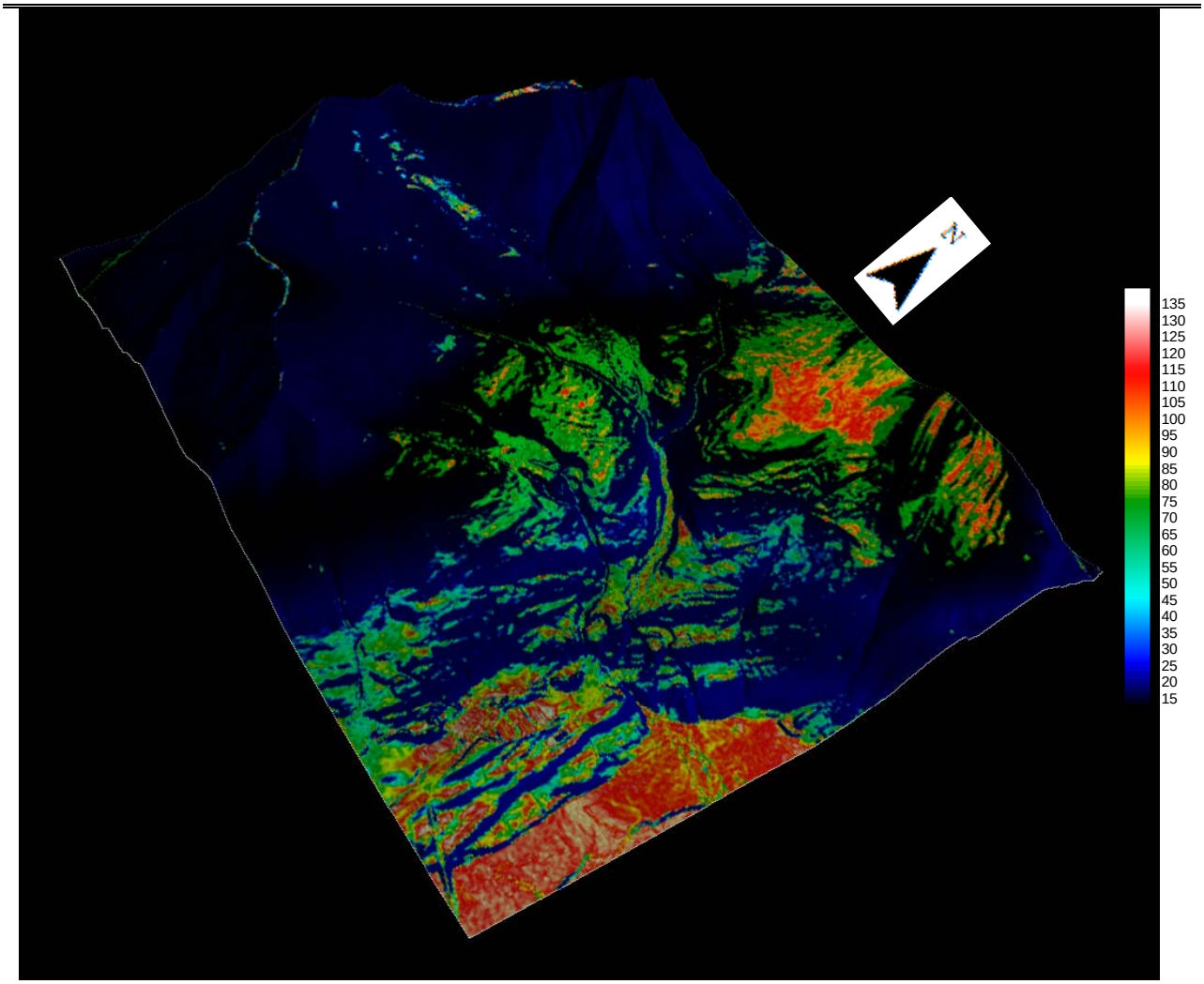

Figure 8 illustrates the incoming solar radiation for July 1st, 2008. Even during the middle of the summer shading is evident along the ridge top. Note again the higher insolation values in the valley bottom.

Figure 8: Liston model with the LLRA lapse rate utilizing Spline interpolation; Date : July 01, 2008 14:00; Units = W/m^2

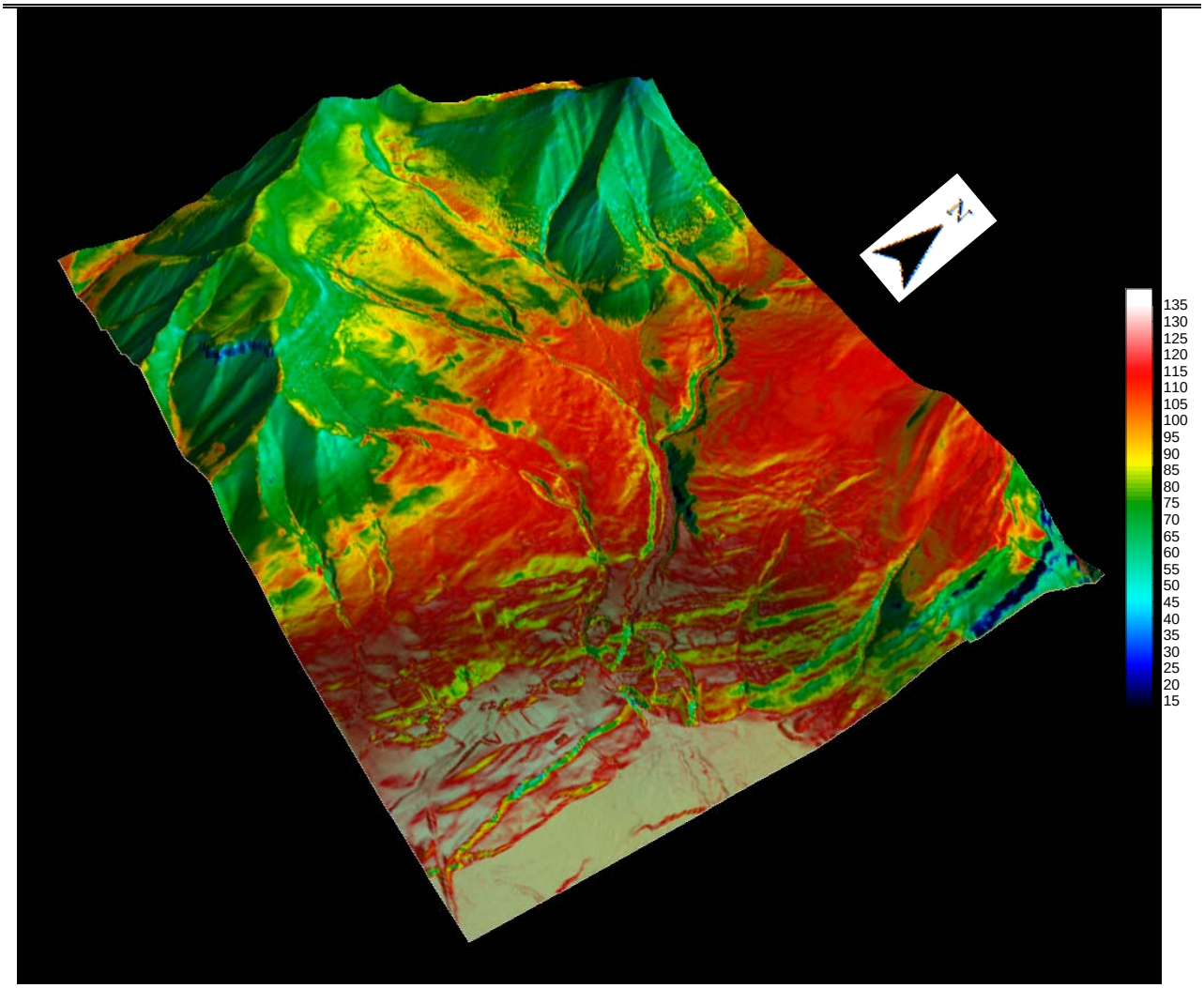

Figures 9-12 show the comparisons of the Annandale (ANA) method and the Campbell-Bristow-Walter (CBW) method. In sharp contrast to the figure above, the interpolation method has a significant effect on the output. The 'wells' essentially mark the influence of a single station. As is evident upon comparison of the figures, spline, as noted above, does a significantly better job at reducing these wells and creating a smoother dataset. Much like the Liston method above, the short wave radiation values in the valley are higher than on the ridge. If, as per the third hypothesis above, the ridges favour cloud formation, this would result in a smaller difference in minimum and maximum air temperature, which the model interprets as "cloudy". Since these methods do not incorporate terrain slope and aspect, the terrain shading hypothesis as per above are not applicable here.

Figure 9: CBW IDW Jan 1 Units of W/m^2

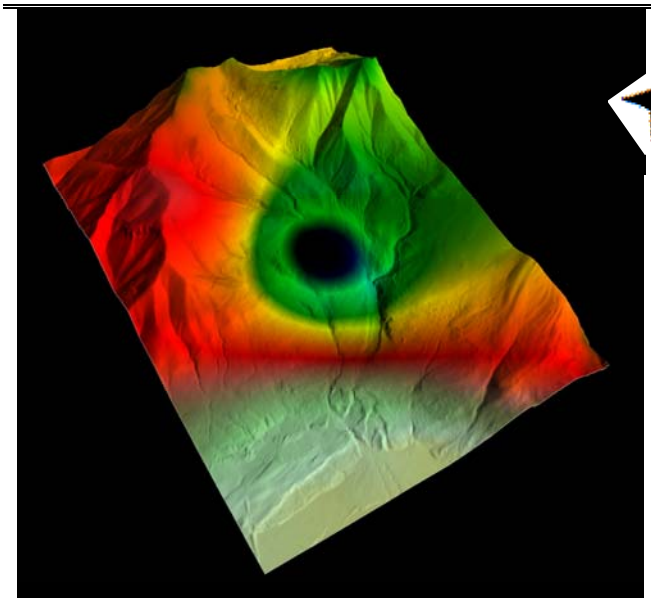

Figure 10: CBW Spline Jan 1 Units of W/m^2

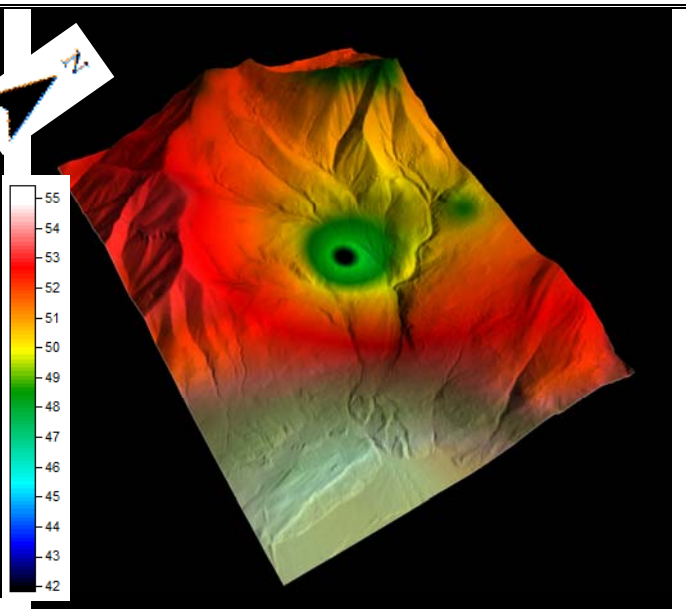

Figure 11: ANA IDW Jan 1 Units of W/m^2

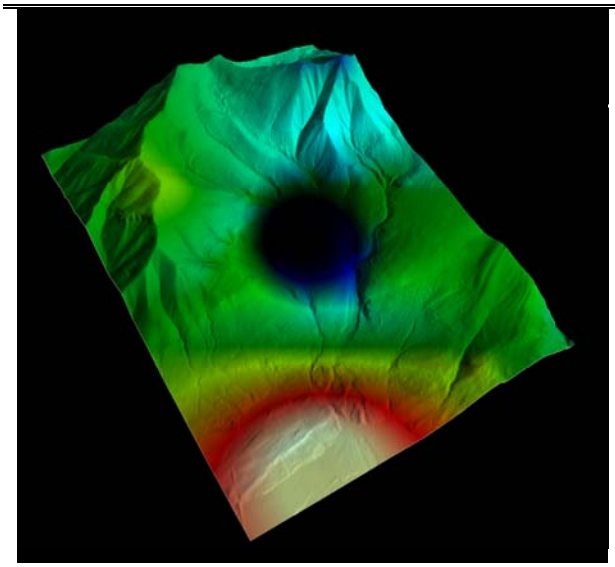

Figure 12: ANA Spline Jan 1 Units of W/m^2

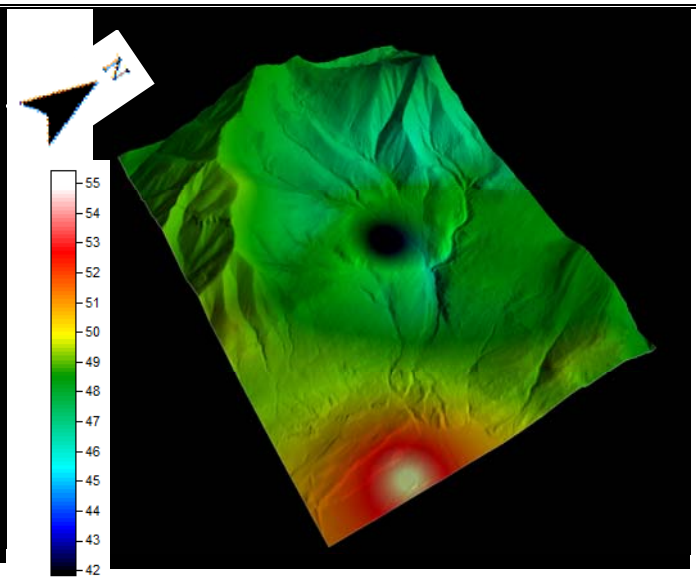

Figures 13 through 16 are for July 1st, 2008. Again, the interpolate has a very large effect on the resulting outcome with spline having the most accurate interpolation.

Figure 13: CBW IDW Jul 1 Units of W/m^2

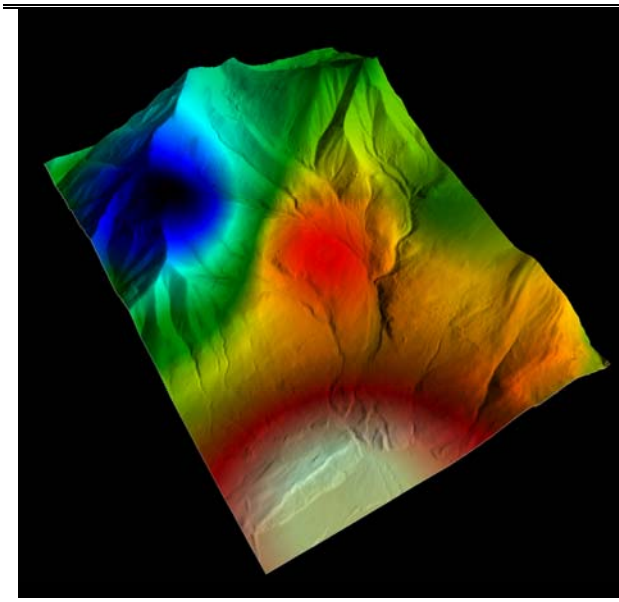

Figure 14: CBW Spline Jul 1 Units of W/m^2

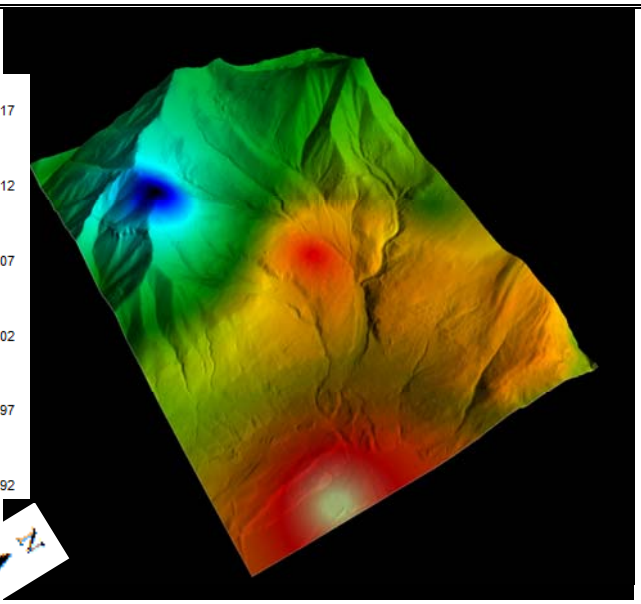

Figure 15: ANA IDW Jul 1 Units of W/m^2

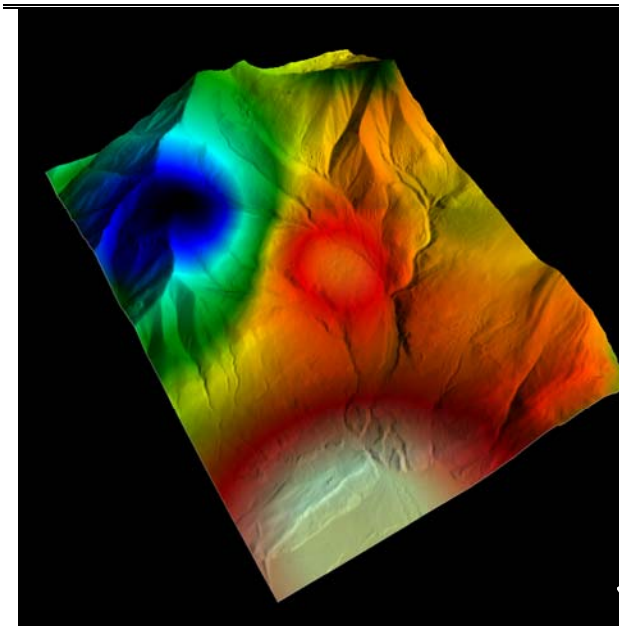

Figure 16: ANA Spline Jul 1 Units of W/m^2

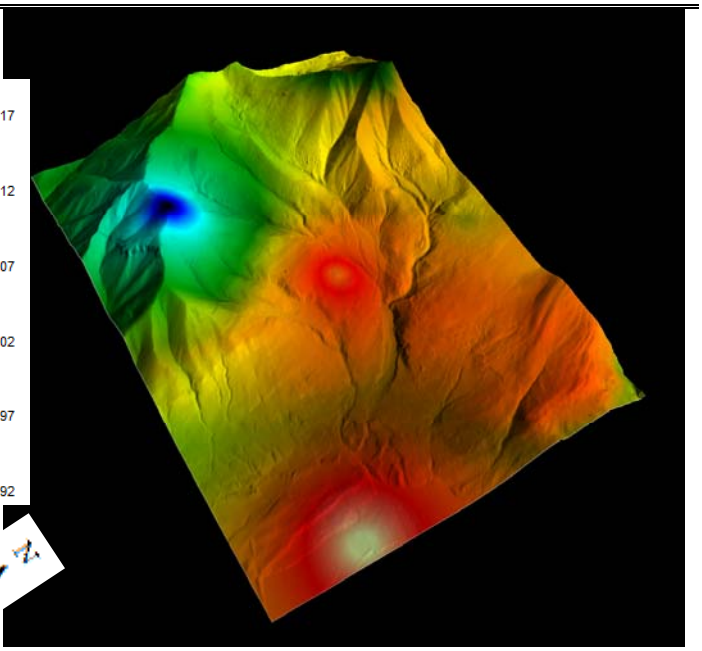

Figure 17 demonstrates the output from ArcGIS Solar Analyst for January and July 1st, 2008 at 14:00. Due to its very complex viewshed generation, the spatial variability is very high and is very sensitive to the underlying topographic features. Note that unlike Liston's model, the Solar Analyst has more incoming shortwave onto the south facing portion of the ridge (top left of 3D model) which is a much more accurate spatial prediction.

Figure 17 ArcGIS Solar Analyst output. Jan 1st, 2008. 14:00. Units of W/m^2

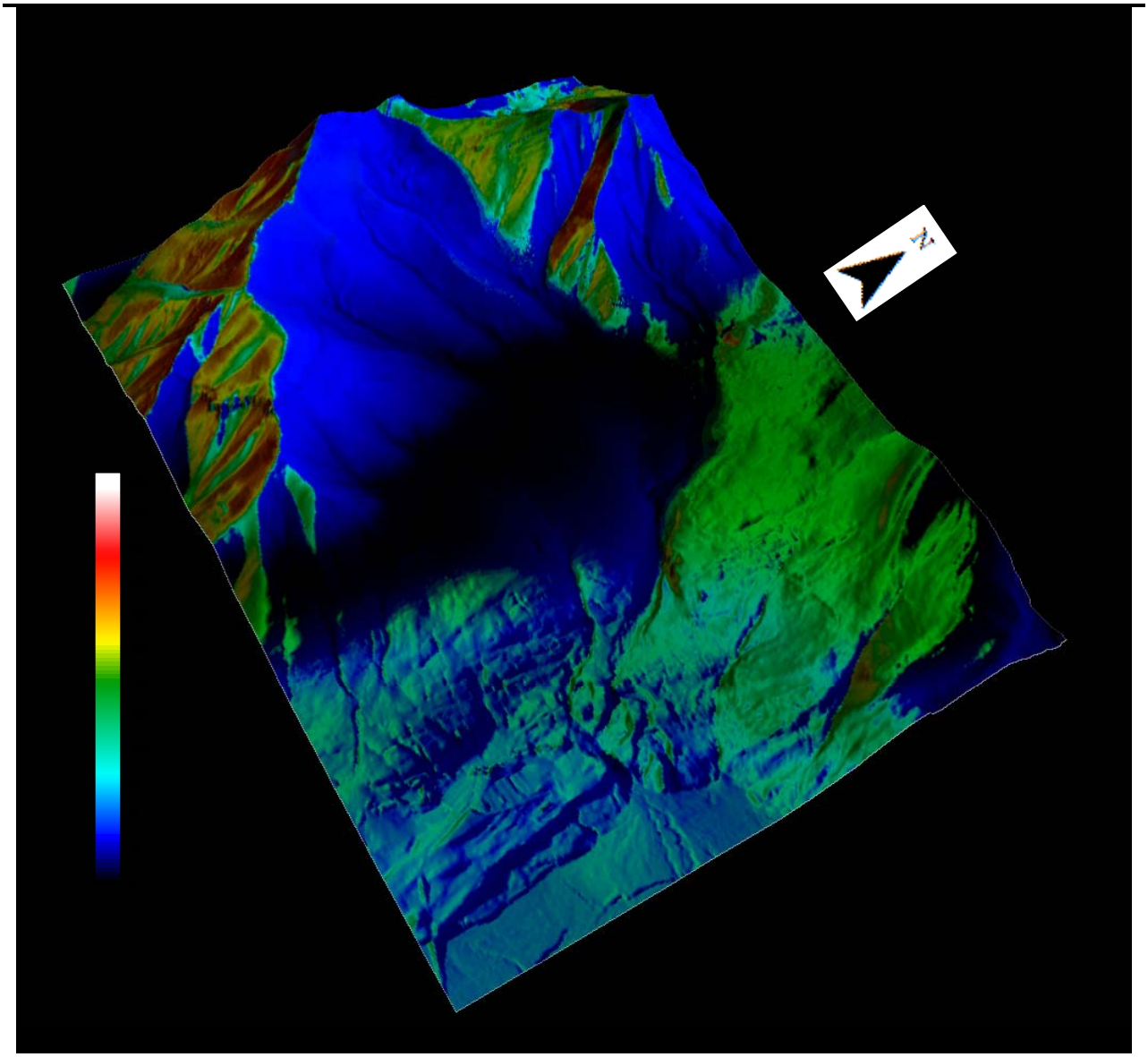

Figure 18 is again ArcGIS output, for July 1st, 2008 at 14:00. There is a significant difference compared to the output of from the Liston and Elder implementation. The ridge has significant differences, especially the back side (south facing) which has more insolation. This is a more realistic representation of the situation, as the Liston and Elder model has both sides shaded. The model does suffer from having higher values in the valley; however this is again due to the lack of shading from the ranges to the east.

Figure 18. ArcGIS Solar Analyst output. Jul 1st, 2008. 14:00. Units of W/m^2

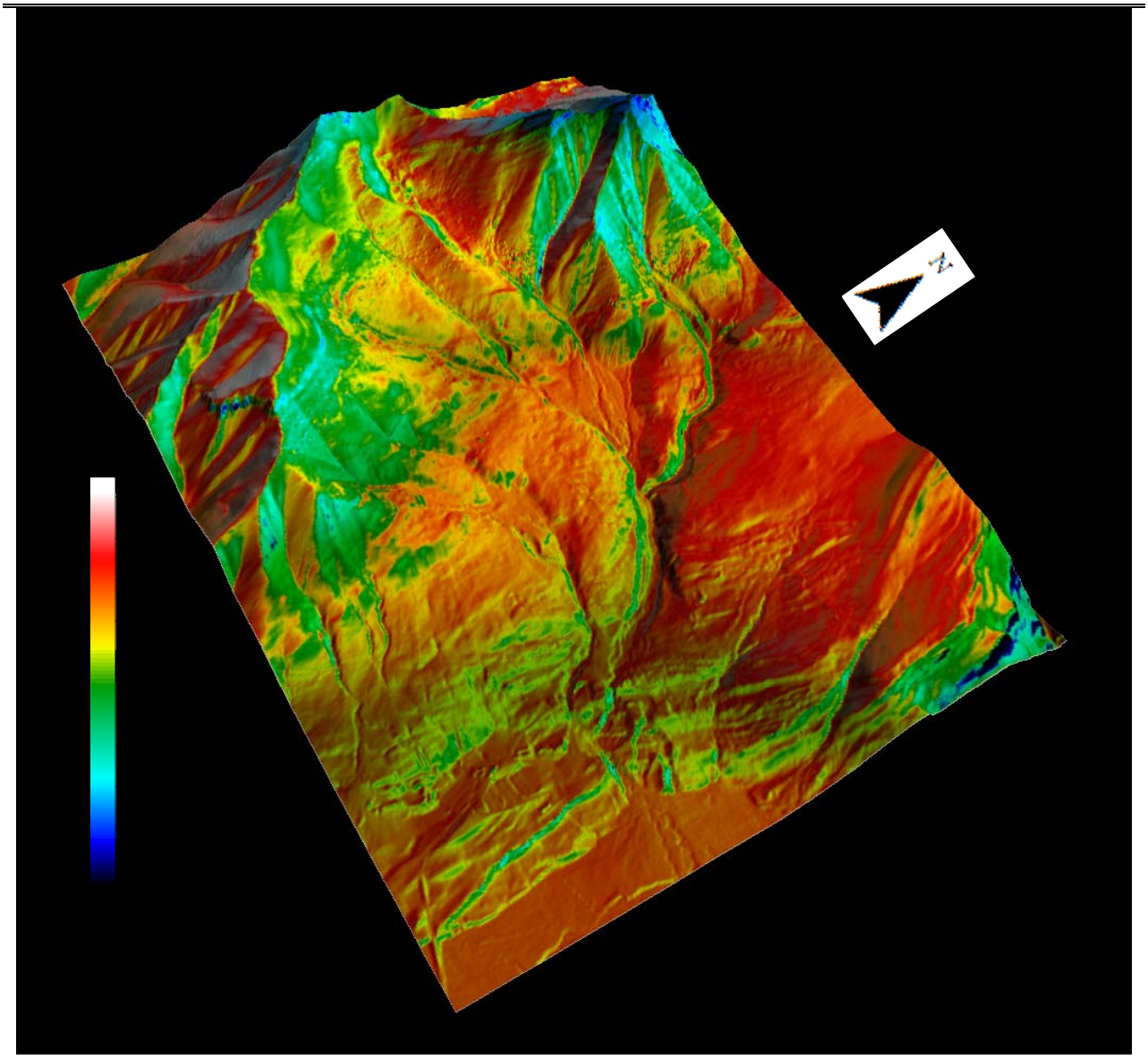

Figures 19 illustrates the LLRA, spline interpolation of temperature. Notice how the spline interpolate has smoothed out the data and the wells present in 13-16 are not a factor here. It exhibits strong elevational banding, as expected.

Figure 19. Air temperature (^{o}C) July 1st, 2008 at 14:00

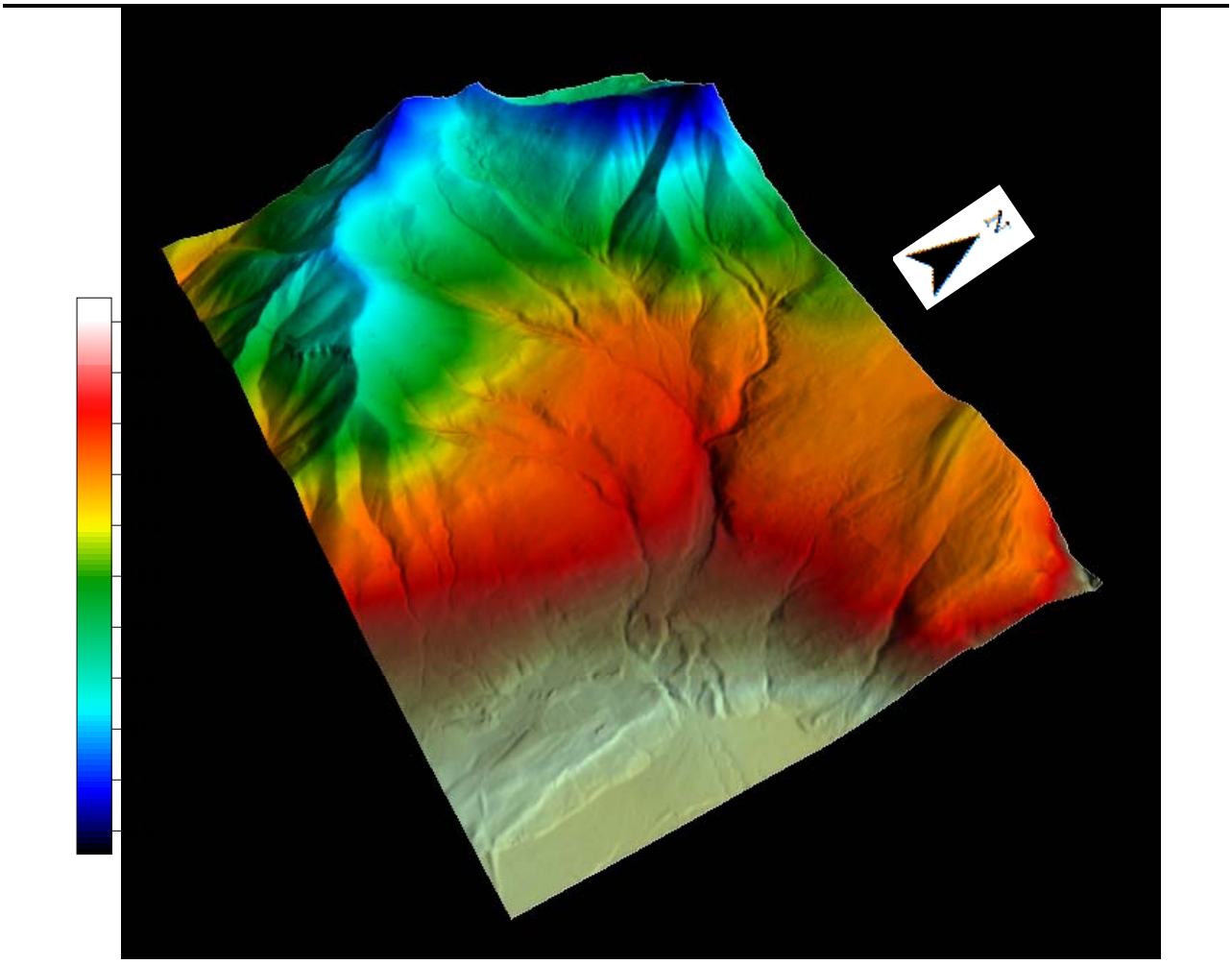

8. C O N C L U S I O N

Meteorological variables were distributed over a model domain in the Canadian Rockies and were used to estimate incoming solar radiation. To achieve the spatial interpolation, two spatial interpolation methods were evaluated; inverse distance weighting and thin-plate splines with tension. Incoming solar radiation was calculated using an empirical equation, a quasi-physically based equation and a physically based equation with "average" parameters (such as transmittance). The empirical models utilized only air temperature differences and the quasi-physically based method utilized actual air temperature and an extrapolated relative humidity at the 700mb level (taken as 3000m).

The empirical insolation methods performed surprisingly well given the lack of a shading algorithm and lack of knowledge of terrain slope and azimuth. However, these methods fail for any location that experiences frequent shading or is significantly affected by terrain slope. They are very sensitive to the interpolation method used and utilizing a computationally expensive gridding method such as thin-plate splines with tension produces significantly better results. Large 'wells' can form around the stations resulting in odd, unrealistic patterns. Using a smoothing interpolate such as splines helps alleviate this. However this comes at a significant runtime cost which increases with the number of stations utilized. The quasi-physically based method performed quite well and was not very sensitive to the gridding method used. Moving from the simple IDW to the thin-plate splines interpolate had a huge runtime cost penalty and given the marginal benefits in utilizing the thin-plate splines, one should probably use IDW. However, if a large domain was examined or had a large site density, it would be worthwhile to revisit the sensitivity as the splines are increasingly powerful with high station density. This is not to say that two stations side by side are better; rather that two stations farther apart can lead to significant improvements when accounting for the spatial variability. The method in the ArcGIS Desktop Solar Analyst toolkit is surprisingly accurate given the complete lack of meteorological forcing data. However, given this lack, it fails to properly account for the seasonal variances in the mountains. As well, there was a very strange artifact in the output data that could not be accounted for. Although this method can be calibrated in a site-specific way, it was run "as-is" to simulate a case where a general approximation of the insolation would be needed. If the data was present to properly calibrate the model, other methods would probably be more suitable and be much less computationally expensive. However, it does capture the topographic effects better than any other method and with improvements such as utilizing a cloud cover fraction like that of Liston and Elder, it may be an extremely powerful option in complex terrain where knowledge of the topographic effects are needed and only limited atmospheric variables are present. Locations in highly vegetated locations are not well represented by any of these

model and a vegetation shading model would need to be included to more accurately represent these locations. In complex terrain, it is important to include the topographic characteristics of the basin, such as slope, aspect and areas of shading. However, in areas such as Marmot Creek where there is shading from outside of the model domain, running the model on a larger extent than used in this study would result in improved predictions. Although it adds significant computational costs, the shading of the surrounding topography on the model domain can result in more accurate results.

Air temperature was distributed using two lapse rates; a monthly variable constant lapse rate and a neutral stability algorithm. Although both performed well, the linear lapse rate performed the strongest. This is thought to be due to the violation of the atmospheric stability assumption as the atmosphere in the mountains especially around the ridges is very unstable due to orographic lift and other such processes. These values are highly sensitive to the interpolation technique used and the computational costs of the spline method are worthwhile, as the results demonstrate much smoother results without the wells that are present in the IDW method. However, due to the smoothing of the data, point value fluctuations are not captured as well as by the IDW method. Investigations into the sensitivity of the temperature to the tension weights and basis function would be needed to fully quantify which spline method would be the best.

Relative humidity performed surprisingly poorly and was the least well modeled of the variables. Its spatial pattern was affected by the interpolate method, in the same manner as air temperature and an over smoothing effect was noticed. The equations that were used for the RH were derived from the Cascade Mountains, U.S.A and Kunkel (1988) noted that "…care must be taken when applying this method to stations located in regions where rapid spatial changes in climate are present". Although the Liston model did not seem to be heavily affected by the poor RH prediction, there is a good chance that if better RH values could be estimated that the shortwave radiation values obtained through Liston and Elder's model would produce more accurate results.

In general the empirical methods provided a good overall daily prediction, however they over predicted the values in areas which experienced high levels of shading. Utilizing a smoothing spatial interpolate such as thin-plate spline with tension proved to be the best option. Further work needs to be done to fully examine the effect of the smoothness on the data. Physically based terrain shading methods provided significantly more reliable predictions, however the lack of shading inclusion from outside the basin resulted in higher than measured values in locations such as the valley which would normally experience terrain shading. Without site-specific atmospheric forcing data, general "average" value method fail to capture the highly variable insolation and end up highly over predicting the values.

9. A C K N O W L E D G E M E N T S

The author would like to thank the following individuals for their help on this project: John Pomeroy, Kevin Shoot, Mike Solohub and Matt MacDonald. The author is thankful for the data that was provided for this project by the Centre for Hydrology at the University of Saskatchewan.

10. R E F E R E N C E S

Annandale, J. G., N.Z. Jovanic, N. Benade, and R. G. Allen. 2002. Software for missing data error analysis of Penman-Monteith reference evapotranspiration. *Irrigation Science* 21, no. 2: 57-67.

Bolstad, Paul V., Lloyd Swift, Fred Collins, and Jacques Régnière. 1998. Measured and predicted air temperatures at basin to regional scales in the southern Appalachian mountains. *Agricultural and forest meteorology* 91: 161-176.

Bristow, Keith L., and Gaylon S. Campbell. 1984. On the relationship between incoming solar radiation and daily maximum and minimum temperature. *Agricultural and forest meteorology* 31, no. 2: 159-166.

---. 1985. An equation for separating daily solar irradiation into direct and diffuse components. *Agricultural and forest meteorology* 35: 123-131.

Chang, Kang-tsung. 2008. *Introduction to Geographic Information Systems*. McGraw Hill.

Chung, Uran, and Yin I. Yun. 2004. Solar irradiance-corrected spatial interpolation of hourly temperature in complex terrain. *Agricultural and Forest Meteorology* 126: 129-139.

Dodson, Rusty, and Danny Marks. 1997. Daily air temperature interpolated at high spatial resolution over a large mountainous region. *Climate Research* 8: 1-20.

Environmental Systems Research Institute, Inc. 2008. ArcGis 9.3 student edition - help manual.

Evrendilek, Faith, and Can Ertekin. 2008. Assessing solar radiation models using multiple variables over Turkey. *Climate dynamics* 31: 131-149.

Fu, P, and P.M Rich. 2002. A geometric solar radiation model with applications in agriculture and forestry. *Computers and Electronics in Agriculture* 37: 25-35.

Garnier, B. J., and Atsumu Ohmura. 1968. A method of calculating the direct shortwave radiation income of slopes. *Journal of Applied Meteorology* 7: 796-800.

Kunkel, Kenneth E. 1988. Simple Procedures for Extrapolation of Humidity Variables in the Mountainous Western United States. *Journal of Climate* 2: 656-669.

List, R. J. 1968. *Smithsonian Meterological Tables*. Vol. 6. Smithsonian Institute.

Liston, Glen E., and Kelly Elder. 2006. A meteorological distribution system for high-resolution terrestrial modeling (MicroMet). *Journal of hydrometeorology* 7: 217-234.

Marks, Danny. 1990. A continental-scale simulation of potential evapotranspiration for historical and projected doubled-CO2 climate conditions. In *Biospheric feedbacks to climate change: the sensitivity of regional trace gas emissions, evapotranspiration, and every balance to vegetation redistribution. EPA/600/3-90/78*. U.S. Environmental Protection Agency, Corvallis.

Mitasova, H, and L Mitas. 1993. Interpolation by Regularized Spline with Tension: I Theory and Implementation. *Mathematical Geology* 25: 641-655.

Myers, Donald E. 1993. Spatial interpolation: an overview. *Geoderma* 62, no. 1-3: 17-28.

Nash, J.E, and J. V. Sutcliffe. 1970. River flow forecasting through conceptual models part I — A discussion of principles. *Journal of Hydrology* 10, no. 3: 282-290.

Oliphant, A. J., R.A. Spronken-Smith, A. P. Sturman, and I. F. Owens. 2003. Spatial variability of surface radiation fluxes in mountainous terrain. *Journal of Applied Meteorology* 42: 113-128.

Ranzi, Roberto, and Renzo Rosso. 1995. Distributed estimation of incoming direct solar radiation over a drainage basin. *Journal of Hydrology* 166: 461-478.

Rich, P.M., R Dubayah, W.A Hetrick, and S.C. Saving. 1994. Using Viewshed models to calculate intercepted solar radiation: applications in ecology. *American Society for Photogrammetry and Remote Sensing Technical Papers*: 524-529.

Rosenberg, Norman J., Blaine L. Blad, and Shashi B. Verma. 1984. *Microclimate: The Biological Environment*. New York: Wiley.

Shook, Kevin, and John Pomeroy. 2008. Analysis of Synthetic Shortwave Solar Radiation Datasets for Hydrological Simulation on the Canadian Prairies. *Work in progress*.

Thornton, Peter E, Hubert Hasenauer, and Micheal White. 2000. Simulaneous estimation of daily solar radiation and humidity from observed temperature and precipitaion: an application over complex terrain in Austria. *Agricultural and Forest Meteorology*, no. 104: 255-271.

Thornton, Peter E., and Steven W. Running. 1999. An improved algorithm for estimating incident daily solar radiation from measurements of temperature, humidity and precipitation. *Agricultural and Forest Meteorology*, no. 93: 211-228.

Wallace, John M., and Peter V. Hobbs. 2006. *Atmospheric Science: An introductory survey*. Academic Press.

Walter, M. Todd, Erin S. Brooks, Donal K. McCool, Larry G. King, Myron Molnau, and Jan Boll. 2005. Process-based snowmelt modeling: does it require more input data than temperature-index modeling? *Journal of Hydrology* 300: 65-75.

Weiss, Albert, Cynthia J. Hays, Qi Hu, and William E. Easterling. 2001. Incorporating Bias Error in Calculating Solar Irradiance: Implications for Crop Yield Simulations. *Agronomy Journal* 93, no. November-December.

Young, Andrew T. 1994. Air mass and refraction. *Applied optics* 33, no. 6: 1108-1110.